Article

Current Biology

Dynamic REM Sleep Modulation by Ambient Temperature and the Critical Role of the Melanin-Concentrating Hormone System

Graphical Abstract

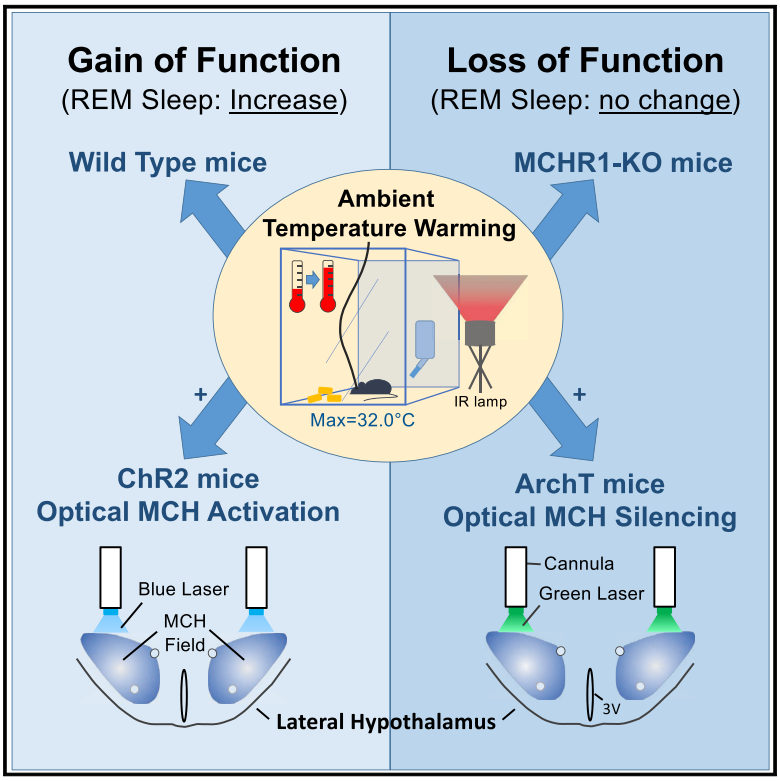

Authors

Noëmie Komagata, Blerina Latifi, Thomas Rusterholz, Claudio L.A. Bassetti, Antoine Adamantidis, Markus H. Schmidt

Correspondence

markus.schmidt@insel.ch

In Brief

The control and function of temperature-induced REM sleep modulation have remained unknown. Komagata et al. show that the melanin-concentrating hormone system within the lateral hypothalamus plays a critical role in the dynamic ability of the organism to opportunistically increase REM sleep when the need for core body temperature defense is minimized.

Highlights

- Wild-type mice dynamically increase REM sleep with ambient temperature (T_a) warming
- Optogenetic MCH activation overdrives REM sleep expression during T_a warming
- Optogenetic MCH silencing or lack of MCH receptor blocks T_a modulation of REM sleep
- The MCH system plays a critical role in modulating REM sleep as a function of T_a

Komagata et al., 2019, Current Biology *29*, 1976–1987
June 17, 2019
https://doi.org/10.1016/j.cub.2019.05.009

CellPress

CellPress

Current Biology
Article

Dynamic REM Sleep Modulation by Ambient Temperature and the Critical Role of the Melanin-Concentrating Hormone System

Noëmie Komagata,[1] Blerina Latifi,[1] Thomas Rusterholz,[2] Claudio L.A. Bassetti,[3] Antoine Adamantidis,[2,4] and Markus H. Schmidt[2,3,5,6,*]

[1]Bern University Hospital (Inselspital), University of Bern, 3010 Bern, Switzerland
[2]Center for Experimental Neurology, Department of Neurology, Bern University Hospital (Inselspital), University of Bern, 3010 Bern, Switzerland
[3]Department of Neurology, Bern University Hospital (Inselspital), University of Bern, Freiburgstrasse 18, 3010 Bern, Switzerland
[4]Department of Biomedical Research (DBMR), Bern University Hospital (Inselspital), University of Bern, 3010 Bern, Switzerland
[5]Ohio Sleep Medicine Institute, 4975 Bradenton Avenue, Dublin, OH 43017, USA
[6]Lead Contact
*Correspondence: markus.schmidt@insel.ch
https://doi.org/10.1016/j.cub.2019.05.009

SUMMARY

Ambient temperature (T_a) warming toward the high end of the thermoneutral zone (TNZ) preferentially increases rapid eye movement (REM) sleep over non-REM (NREM) sleep across species. The control and function of this temperature-induced REM sleep expression have remained unknown. Melanin-concentrating hormone (MCH) neurons play an important role in REM sleep control. We hypothesize that the MCH system may modulate REM sleep as a function of T_a. Here, we show that wild-type (WT) mice dynamically increased REM sleep durations specifically during warm T_a pulsing within the TNZ, compared to both the TNZ cool and baseline constant T_a conditions, without significantly affecting either wake or NREM sleep durations. However, genetically engineered MCH receptor-1 knockout (MCHR1-KO) mice showed no significant changes in REM sleep as a function of T_a, even with increased sleep pressure following a 4-h sleep deprivation. Using MCH-cre mice transduced with channelrhodopsin, we then optogenetically activated MCH neurons time locked with T_a warming, showing an increase in REM sleep expression beyond what T_a warming in yellow fluorescent protein (YFP) control mice achieved. Finally, in mice transduced with archaerhodopsin-T, semi-chronic optogenetic MCH neuronal silencing during T_a warming completely blocked the increase in REM sleep seen in YFP controls. These data demonstrate a previously unknown role for the MCH system in the dynamic output expression of REM sleep during T_a manipulation. These findings are consistent with the energy allocation hypothesis of sleep function, suggesting that endotherms have evolved neural circuits to opportunistically express REM sleep when the need for thermoregulatory defense is minimized.

INTRODUCTION

Rapid eye movement (REM) sleep is characterized by a well-described, but poorly understood, association with thermoregulatory neurophysiology. In addition to the cortical activation, generalized skeletal muscle atonia, and rapid eye movements that define this sleep state, a striking feature of REM sleep is the concomitant loss of thermoregulatory control [1–4]. Across endotherms examined, panting, piloerection, sweating, or shivering are maintained in NREM sleep and wakefulness, but these thermoregulatory defenses cease in REM sleep, as seen when sleeping in ambient temperatures (T_a) deviating from thermoneutrality [1–4]. The thermoneutral zone (TNZ), or thermoneutrality, is defined by a narrow T_a range where resting metabolic rate remains stable. Metabolic rate will increase, however, as the T_a deviates from thermoneutrality, primarily due to activation of thermoregulatory responses.

The function of thermoregulatory loss during REM sleep has remained unknown. The energy allocation (EA) hypothesis of sleep specifically addresses this question, postulating that REM sleep is a behavioral strategy that orchestrates a shift in energy resources away from the periphery and thermoregulatory defense toward, instead, the CNS [5–7]. Thermoregulation is the most expensive biological function encountered by endotherms [8, 9], i.e., species that maintain a constant body temperature. The EA hypothesis proposes that endotherms have evolved to opportunistically express REM sleep when the need for thermoregulatory defense is minimized or, rather, to sacrifice REM sleep when thermoregulatory defense is required [5, 7]. This hypothesis predicts the presence of neural mechanisms to dynamically modulate REM sleep expression as a function of T_a.

Although both NREM and REM sleep are promoted by thermoneutral warming, REM sleep expression is more sensitive to T_a manipulation than NREM sleep [3, 10–13]. For example, even

though NREM sleep durations remain relatively stable when T_a is manipulated within the TNZ during the circadian sleep phase, REM sleep durations can increase by as much as 2-fold as the T_a is warmed from the low to high end of the TNZ [10, 11]. Moreover, analyses of the cycling of NREM and REM sleep suggest that the inter-REM intervals may lengthen with T_a cooling and shorten with T_a warming, even in human subjects [3, 14]. These and other data further show that, as ambient temperatures deviate from thermoneutrality, REM sleep expression precipitously declines and either wakefulness or NREM sleep are favored [4, 15, 16], likely as a mechanism to promote robust thermoregulatory defenses.

The anterior hypothalamus plays an important role in both thermoregulation and NREM sleep generation [17–22], but the control of REM sleep during T_a manipulation remains unknown. We hypothesize that melanin-concentrating hormone (MCH) neurons in the posterior lateral hypothalamus (LH) may be a potential candidate for this REM sleep control. Indeed, experimental approaches employing optogenetic [23–25], chemogenetic [26, 27], and pharmacologic [28–30] interventions have consistently demonstrated that the MCH system promotes REM sleep expression. However, all prior work on the MCH system has been performed at constant temperature conditions.

To test the hypothesis that the MCH system drives the dynamic modulation of REM sleep as a function of T_a, MCH receptor-1 knockout (MCHR1-KO) and MCH-cre mice were exposed to rapid warm temperature pulsing toward the high end of the mouse TNZ. The TNZ range for the adult mouse is approximately 25°C–33°C [31, 32]. We show that wild-type (WT) mice significantly and dynamically increased REM sleep durations during warm T_a pulsing toward 32°C, an effect absent in MCHR1-KO mice. Optogenetic manipulation of MCH neurons confirmed a critical role for the MCH system in modulating REM sleep expression as a function of T_a. These findings have important evolutionary implications regarding the function of REM sleep and are consistent with fundamental principles of the EA hypothesis of sleep function.

RESULTS

Following control recordings at a constant 23.0°C ± 1.0°C, mice were habituated to daily warm temperature pulsing using a combination of convection heater and infrared lamp (see Figure 1A and STAR Methods). This protocol produced four 60-min bins in the light period during which the T_a increased to ~32.0°C (mean = 28.5°C), i.e., the high end of the mouse TNZ (TNZ warm condition; Figure 1B). During passive cooling, the TNZ warm periods were followed by four 60-min bins where the T_a decreased to an average of approximately 25.6°C (TNZ cool condition).

As shown in Figure 1C, WT mice demonstrated a significant increase in total REM sleep duration during the TNZ warm condition compared to the control and TNZ cool conditions, an effect not observed in MCHR1-KO mice (interaction $F_{(2,34)} = 12.24$; $p < 0.0001$). During the TNZ warm condition, WT mice showed a significant increase in the number of REM sleep bouts (Figure 1D; T_a-condition $F_{(2,34)} = 4.18$, $p = 0.0238$; interaction $F_{(2,34)} = 5.574$, $p = 0.0081$) and a significant decrease in the inter-REM intervals (Figure 1E; T_a-condition $F_{(2,34)} = 9.704$; $p = 0.0005$) but with no significant change in the mean REM sleep bout duration (Figure 1F). MCHR1-KO mice, in contrast, showed no significant changes in any of the REM sleep parameters measured (Figures 1C–1F). Finally, the dynamic temperature manipulations did not produce any significant changes in NREM sleep or wake durations across conditions in either WT or MCHR1-KO mice (Figure S1A). Spectral analyses of the electroencephalogram (EEG) in WT mice demonstrated that the EEG in both REM sleep and NREM sleep remained unchanged during T_a warming compared to the control (23.0°C ± 1.0°C) condition (Figure S1B).

To evaluate a potential circadian effect, the warm temperature pulsing experiments were repeated during the dark circadian phase in WT mice using the same parameters. Dynamic T_a pulsing during the circadian dark phase resulted in no significant changes in the quantities of REM sleep, NREM sleep, or wake across conditions (Figure S1C). These data demonstrate that the effects on REM sleep expression from T_a warming are specific to the light (inactive) circadian phase.

Brain temperatures (T_b) in WT mice remained unchanged during T_a warming compared to the control (constant T_a) condition. However, T_b showed a small but significant decrease during the passive cooling phase of the TNZ cool versus control condition (Figure 1G). We speculate this decrease in T_b to be secondary to a compensatory vasodilatation of the skin vasculature triggered by the TNZ warm phase, leading to heat loss during passive cooling in the TNZ cool condition. Importantly, T_b was dependent on behavioral state, showing state-specific rises during both wake and REM sleep and decreases during NREM sleep, irrespective of T_a condition (Figure 1H). Given the dependency of T_b on behavioral state, we further calculated the average T_b for each behavioral state across conditions (Figure 1I). Although there was a trend for waking T_b in the TNZ cool condition to be lower than during constant temperature ($p = 0.078$), there were no significant, state-specific differences in T_b across conditions. Finally, an analysis of T_b across transitions of sleep and wake states also showed no significant differences in T_b between T_a warming and the control temperature condition (Figure S1D).

Taken together, these data demonstrate that WT mice significantly increase REM sleep when the ambient temperature is warmed toward the high end of the TNZ and that the MCH system is implicated in this control, given the absence of this REM-sleep-modulating effect in MCHR1-KO mice. Moreover, the effects of T_a warming are specific to REM sleep during the circadian light (inactive) phase and do not appear to be mediated by changes in T_b.

Sleep Deprivation, Recovery, and the Role of Ambient Temperature

We sought to determine whether increased sleep pressure may rescue the increase in REM sleep expression during the warming phases in MCHR1-KO mice. We also sought to evaluate the potential role of the MCHR1 receptor on sleep recovery as a function of T_a. Following a 4-h total sleep deprivation at constant temperature (23.0°C ± 1.0°C) using gentle handling at the beginning of the light period, mice were allowed to recover sleep at either the constant T_a condition or during exposure to three bouts of warm T_a pulsing as performed in the prior experiment (Figure 2A).

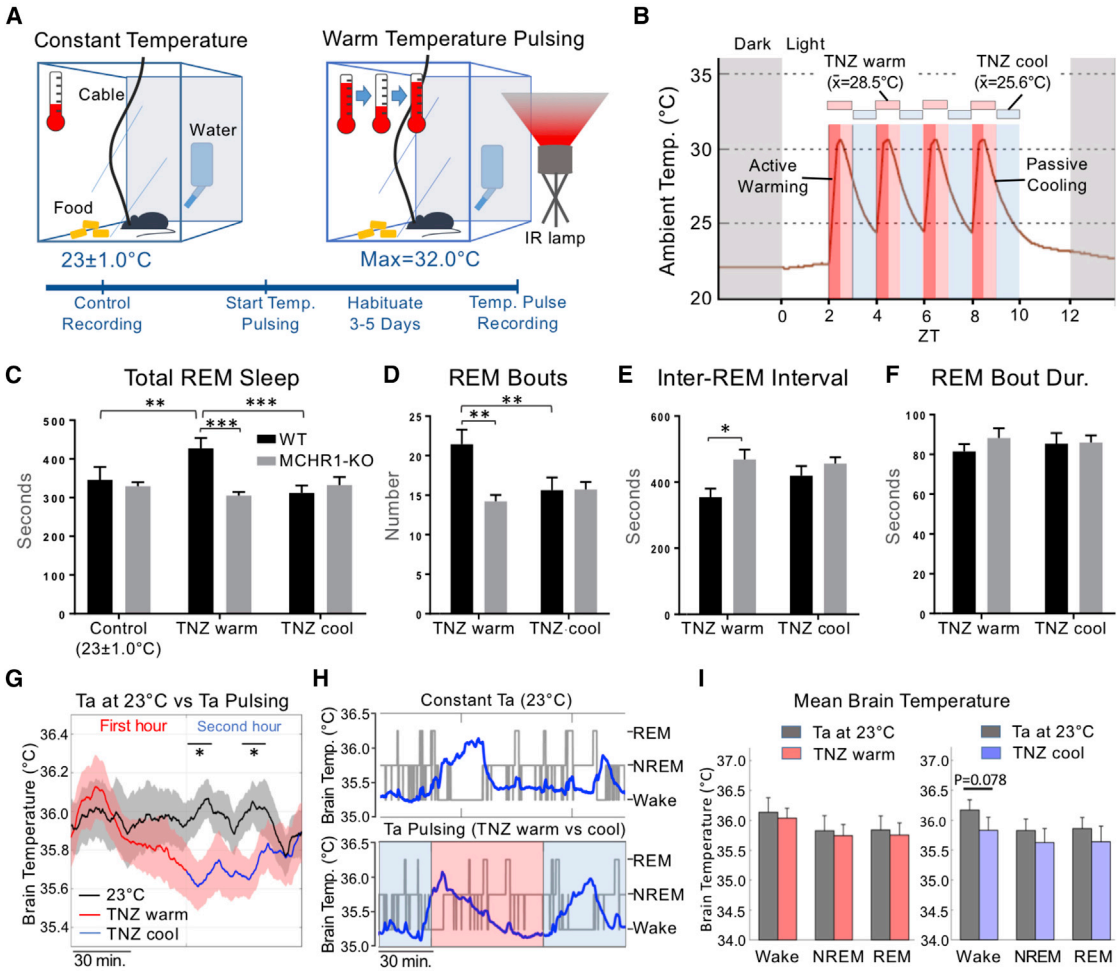

Figure 1. The Effects of Warm Temperature Pulsing on REM Sleep and Brain Temperature

(A) Mice were housed in home cages. Following control recordings at a constant T_a, mice were habituated to warm temperature pulsing.

(B) Four bouts of T_a warming were performed during the light phase at 2-h intervals, providing alternating 60-min bouts of thermoneutral zone (TNZ) warm (red vertical bars; T_a = 27.5°C–32.0°C) and TNZ cool (blue; T_a = 24.5°C–27.5°C) conditions. Dark red vertical bars indicate active warming phase.

(C) Total REM sleep duration was significantly increased in WT mice (n = 8; black) during the TNZ warm condition, an effect not observed in MCHR1-KO mice (n = 11; gray).

(D–F) REM sleep in WT mice during T_a warming showed a significant increase in REM sleep bout number across sessions (D) and a significant decrease in inter-REM intervals (E) but without effect on mean REM sleep bout durations (F).

(G) Mean brain temperature (T_b) from WT mice (n = 4) recorded during either constant T_a (black) condition or during warm T_a pulsing with the TNZ warm phase (red) followed by the TNZ cool phase (blue). There were no significant differences in T_b between control and TNZ warm conditions. During the TNZ cool phase, however, T_b was significantly lower compared to the constant T_a condition (Student's t test).

(H) Raw data of T_b during constant temperature condition (top) and T_a pulsing (below) showing dependency of T_b on behavioral state with typical decreases during NREM sleep and increases during wake and REM sleep.

(I) No significant, state-dependent differences were observed in T_b between the control condition and either the TNZ warm or TNZ cool conditions. However, there was a trend for decreased T_b during wake in the TNZ cool condition (Student's t test; p = 0.078). Unless specified otherwise, data were analyzed using repeated-measures two-way ANOVA and post hoc Sidak's comparison test. Data are means ± SEM. *p < 0.05; **p < 0.01; ***p < 0.001.

See also Figure S1.

WT mice consistently increased REM sleep expression during the TNZ warm phases compared to the TNZ cool phases of recovery sleep, whereas MCHR1-KO mice showed no differences in REM sleep expression as a function of T_a (Figure 2B). The T_a-dependent effect in WT mice was specific to the state of REM sleep with no clear T_a-dependent changes observed in successive bins of the TNZ warm and cool phases with respect to NREM sleep or wake durations during the recovery period (Figure S2A).

During recovery sleep, WT mice demonstrated significantly greater rates of REM sleep cumulation when exposed to warm temperature pulsing compared to MCHR1-KO mice exposed to the same T_a warming conditions or with respect to both groups of mice under the constant temperature condition (Figure 2C; interaction $F_{(33,231)}$ = 2.171; p = 0.0005). This increase in the rate of REM sleep cumulation occurred specifically during the warming phases. As shown in Figure S2B for WT mice, the

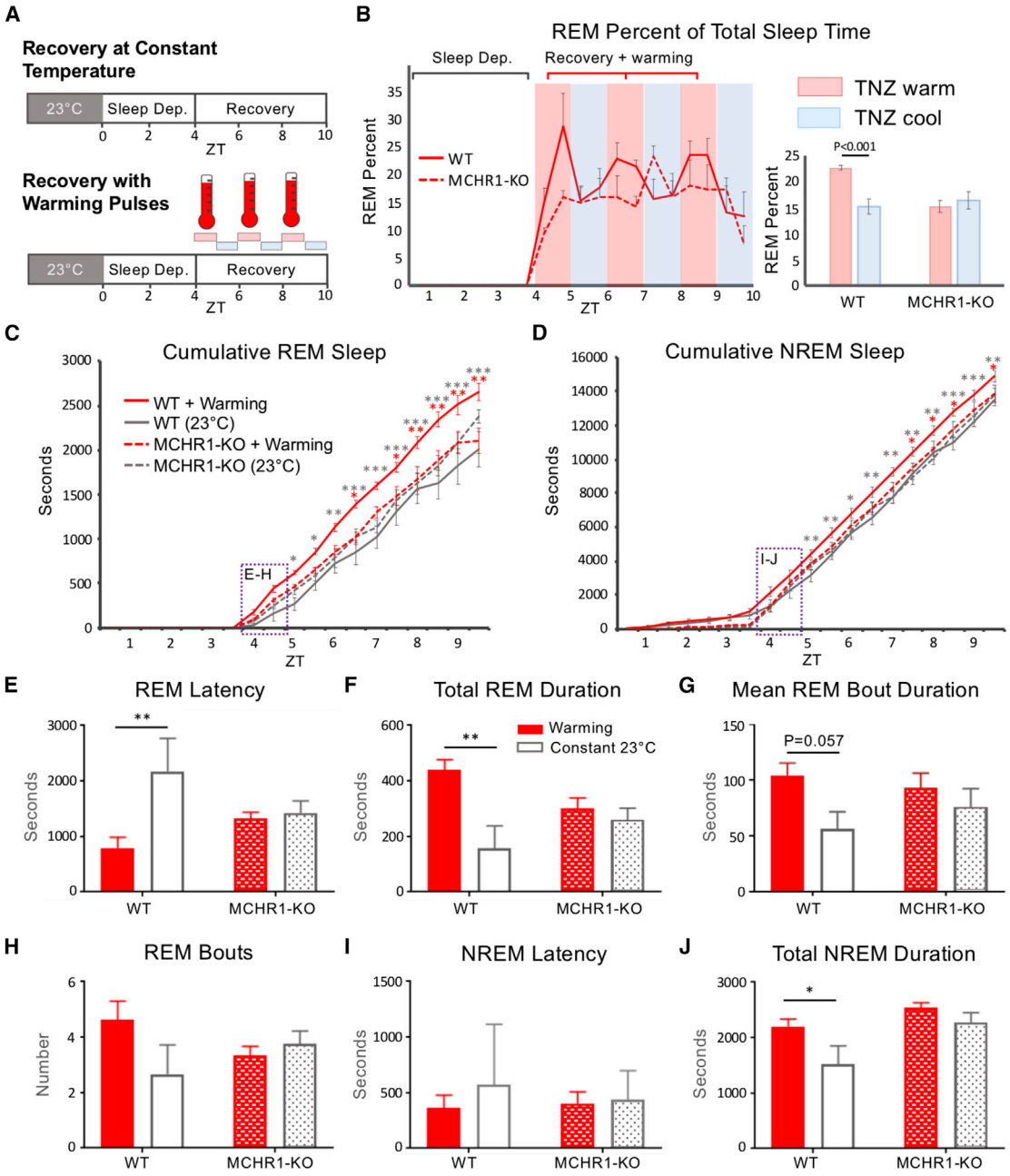

Figure 2. The Effects of Sleep Deprivation on REM and NREM Sleep Recovery as a Function of T_a in WT and MCHR1-KO Mice

(A) Experimental design involving a 4-h sleep deprivation at lights on (zeitgeber time [ZT] 0–4) by gentle handling at constant T_a (23°C), followed by recovery sleep at either constant T_a or with three bouts of warm T_a pulsing.

(B) REM sleep percent of total sleep time (30-min bins) in WT (n = 8) and MCHR1-KO (n = 6) mice during 4-h sleep deprivation and recovery sleep with warm T_a pulsing. WT mice showed increased REM sleep specifically during TNZ warm phases, an effect not seen in MCHR1-KO mice. Aggregate percentage of REM sleep time indicated a significant difference for WT mice during the TNZ warm versus cool condition (Student's t test).

(C and D) Cumulative REM (C) and NREM sleep (D) durations showed significant differences between WT mice exposed to warm T_a pulsing compared to WT mice recovering at constant T_a (black asterisks) and compared to warm T_a pulsing in MCHR1-KO mice (red asterisks).

(E–J) Analyses of the first 60-min of recovery sleep showed significant effects from T_a manipulation only in WT mice for (E) REM sleep latency and (F) total REM sleep duration and (G) a trend for mean REM bout duration. No significant effects from T_a manipulation were observed for (H) number of REM sleep bouts during the first 60 min of recovery sleep. Regarding NREM sleep, no significant effects were observed for (I) NREM sleep latency, but (J) WT mice showed a significant increase in total NREM duration compared to the constant T_a condition. Unless specified otherwise, data were analyzed using repeated measures 2-way ANOVA and post-hoc Sidak's comparison test. Data are means ± SEM. *p < 0.05; **p < 0.01; ***p < 0.001.

See also Figure S2.

slope of REM sleep cumulation during the TNZ warm phases was significantly greater than the slope of REM sleep cumulation during the TNZ cool phases ($p < 0.0001$), a finding not observed in MCHR1-KO mice (Figure S2B). Although WT mice also demonstrated significant differences in the cumulation of NREM sleep (Figure 2D; interaction $F_{(33,231)} = 163.6$; $p < 0.0001$), this NREM sleep effect was primarily driven by a significant increase in total NREM sleep duration during the first hour of recovery (Figure 2J; T_a-condition $F_{(1,21)} = 5.569$, $p = 0.0280$; genotype $F_{(1,21)} = 7.447$, $p = 0.0126$). Importantly, we found no change in the slope of NREM sleep cumulation in the TNZ warm versus cool phases (Figure S2B).

An analysis of the first hour of recovery showed that WT mice dynamically modulated REM sleep expression as a function of T_a during recovery sleep. Compared with the constant T_a condition, WT mice exposed to T_a warming during the first 60 min of recovery showed a significant shortening of the REM latency (Figure 2E; T_a-condition $F_{(1,20)} = 5.955$, $p = 0.0241$; interaction $F_{(1,20)} = 4.473$, $p = 0.0472$), a significant increase in the total REM sleep duration (Figure 2F; T_a-condition $F_{(1,21)} = 0.0058$; interaction $F_{(1,21)} = 5.18$; $p = 0.0334$), and a trend for lengthening the mean REM sleep bout durations (Figure 2G; T_a-condition $F_{(1,19)} = 5.216$, $p = 0.0341$; post hoc comparison for WT group $p = 0.057$) but no significant effect on the total number of REM sleep bouts (Figure 2H). In contrast, MCHR1-KO mice failed to show any significant changes as a function of T_a for REM sleep parameters examined.

Taken together, WT mice following sleep deprivation demonstrated a robust ability to modulate REM sleep expression during recovery sleep as a function of T_a. Although NREM sleep was significantly increased during the first hour of recovery, only REM sleep showed a significant increase in the slope of cumulation during warm temperature pulsing. Finally, mice lacking the MCHR1 receptor were unable to dynamically modulate REM sleep during T_a manipulation, demonstrating that increased sleep pressure does not rescue REM sleep modulation during warm temperature pulsing in MCHR1-KO animals.

Optogenetic MCH Activation

To genetically target the expression of opsins to MCH neurons, we stereotactically injected AAV2-EF1α-DIO-hChR2(H134R)-enhanced yellow fluorescent protein (eYFP) (ChR2) or AAV2-EF1α-DIO-eYFP (YFP) using adeno-associated viruses (AAV2) serotype into the LH of MCH-cre knockin mice as previously described [23]. Baseline recordings were performed at a constant T_a of 23.0°C ± 1.0°C. Experimental conditions involved four 30-min, semi-chronic, optogenetic stimulation sessions occurring either at constant T_a or time locked in combination with the warm T_a pulsing (Figures 3A and 3B).

As shown in Figure 3C, MCH optical activation significantly increased total REM sleep duration over baseline conditions when presented either alone or in combination with warm T_a pulsing (T_a-condition $F_{(2,35)} = 12.73$, $p < 0.0001$; group $F_{(1,35)} = 8.747$, $p = 0.0055$; and interaction $F_{(2,35)} = 3.513$, $p = 0.0407$). YFP control mice, in contrast, only increased REM sleep duration in response to warm temperature pulsing, demonstrating a temperature-specific effect of T_a warming on REM sleep (Figure 3C). No significant effects of optical activation or warm T_a pulsing were observed for NREM sleep or wake in either the ChR2 or YFP animals (Figure S3A). Finally, the increase in REM sleep expression seen in the ChR2 group appeared secondary to an increase in the number of REM sleep bouts (Figure S3B) and with varying effects on mean REM sleep bout durations (Figure S3C) but with no significant effects on the inter-REM intervals (Figure S3D).

MCH optical activation demonstrated a gain of function for REM sleep, showing a significant increase in REM sleep for the ChR2 over the YFP group with either optical stimulation alone or when in combination with warm T_a pulsing (Figure 3D). To better elucidate the timing of the REM sleep effects and to differentiate contributions of laser activation versus T_a warming, a 15-min bin analysis was performed. During optical stimulation at constant temperature, a significant increase in REM sleep percent over baseline was restricted to the ChR2 group specifically during laser activation (Figure 3E). With the addition of T_a warming, laser activation led to a similar increase in REM sleep during the first 30 min in the ChR2 group (Figure 3F). However, following a transient decrease in REM sleep with laser termination, ChR2 mice showed a significant increase in REM sleep during the final 15-min bin of T_a warming (Figure 3F), an effect not observed with laser stimulation alone. In comparison, YFP mice showed significant increases in REM sleep with T_a warming during the second and third 15-min bins of the warming session (Figure 3F).

Anatomical analyses showed double immunohistochemical staining of YFP and MCH neurons within the LH (Figure 3G). A quantification of colocalization demonstrated 80% of all MCH-positive cells were also YFP positive. The transfection of virus was specific to MCH neurons with approximately 2.5% of YFP-positive cells not showing immunohistochemical staining for MCH.

In summary, these data show that MCH optical activation leads to a gain of function in REM sleep expression during T_a warming, exceeding what T_a warming in YFP mice was able to achieve.

MCH Optical Silencing

To determine whether MCH activation is necessary for the increase in REM sleep expression during T_a warming, we stereotactically injected AAV2-EF1α-DIO-ArchT3.0-eYFP (ArchT) or AAV2-EF1α-DIO-eYFP (YFP) using AAV2 viruses into the LH of MCH-cre knockin mice. Similar to the previous experimental protocol design, baseline recordings were performed at a constant T_a of 23.0°C ± 1.0°C, followed by optical silencing at either constant temperature or time locked in combination with T_a warming (Figures 4A and 4B).

YFP control mice significantly increased REM sleep expression specifically during the T_a warming condition, an effect that was blocked by optical MCH silencing in the ArchT group (Figure 4C; interaction $F_{(2,22)} = 3.857$, $p = 0.0366$; T_a-condition $F_{(2,22)} = 6.381$, $p = 0.0065$). Neither MCH silencing nor the combination of ambient temperature manipulation demonstrated any significant effects on NREM sleep or wake durations in either the ArchT or YFP groups (Figure S4A). Compared to ArchT animals, the YFP group demonstrated a significant increase in REM sleep by approximately 27% above baseline during T_a warming (Figure 4D), similar to the degree of REM sleep increase seen in control mice of our prior experiments. This increase in REM sleep during T_a warming in the YFP group was secondary to a relative

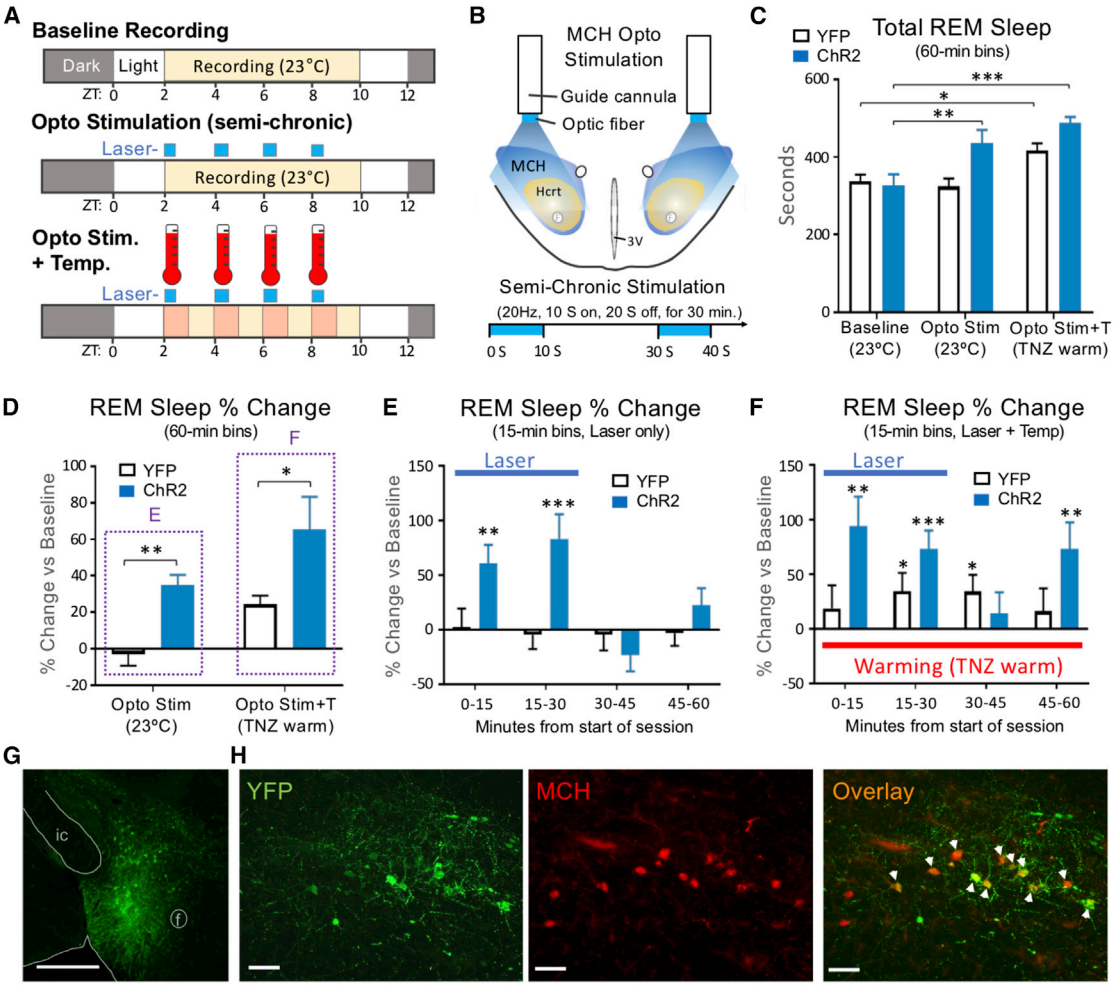

Figure 3. Gain of Function for REM Sleep Expression Resulting from Optical MCH Stimulation during Warm Temperature Pulsing

(A) Three conditions included either the constant T_a for both baseline and MCH optical stimulation (Opto Stim) alone or during four bouts of warm T_a pulsing time locked with MCH stimulation (Opto Stim+T).

(B) Four 30-min bouts of semi-chronic optical stimulations were performed bilaterally using a blue laser (473 nm at 30 mW) in mice transduced with either ChR2 or YFP.

(C) Significant increases in REM sleep were observed following optical stimulation in the ChR2 group (n = 7; blue) either alone (Opto Stim) or in combination with T_a warming (Opto Stim+T), whereas significant increases in REM for the YFP group (n = 7; white) were only observed during the T_a warming condition.

(D) REM sleep percentage change from baseline in 60-min bins for the YFP (white) and ChR2 (blue) groups during the Opto Stim and the Opto Stim+T conditions, showing a gain of function in REM sleep expression in ChR2 mice. The 15-min bin analyses for (E) and (F) are shown in brackets.

(E) During the Opto Stim condition without T_a warming, a 15-min bin analysis showed significant increases in REM sleep percent over baseline for ChR2 mice only during laser activation without significant changes observed in YFP mice.

(F) During the Opto Stim+T condition, a 15-min bin analysis showed significant increases in REM sleep percent over baseline for ChR2 mice not only during laser activation but also during the final 15-min bin during T_a warming after laser termination. The YFP group showed significant increases in REM sleep expression during the second and third 15-min bins during T_a warming.

(G) Overview of YFP expression in posterior LH (approximate anterior-posterior [AP], −1.4 mm).

(H) Photomicrographs show YFP expression (green), MCH neurons (red), and with overlay of double-fluorescence-labeled neurons (white arrowheads). Scale bars: (G) 500 μm; (H) 100 μm.

Data were analyzed in (C) using repeated measures 2-way ANOVA and post-hoc Sidak's comparison test. Two-tailed Student's t tests were performed for (D)–(F). Data are means ± SEM. *p < 0.05; **p < 0.01; ***p < 0.001.

See also Figure S3.

increase in number of REM sleep bouts (Figure S4B; interaction $F_{(2,22)} = 6.678$; $p = 0.0054$) with a significant decrease in the inter-REM intervals (Figure S4C; interaction $F_{(2,22)} = 6.656$; $p = 0.0055$). No significant changes in mean REM sleep bout durations were observed in any condition (Figure S4D).

Although the increase in REM sleep during T_a warming was blocked by MCH silencing, optical silencing in ArchT animals resulted in no significant reductions in REM sleep with respect to baseline conditions during either optical silencing alone (Figure 4E) or in combination with T_a warming (Figure 4F). These

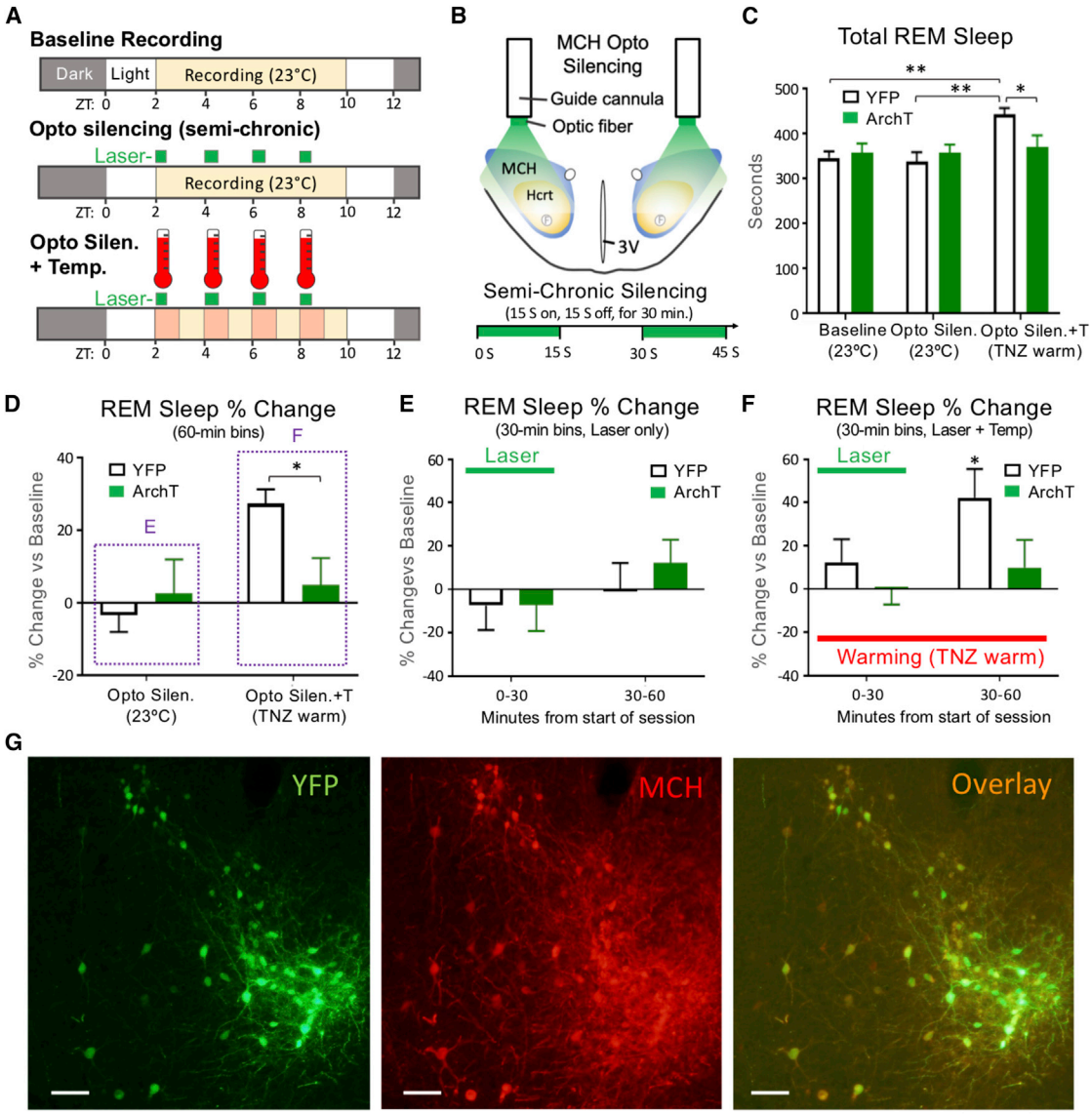

Figure 4. REM Sleep Expression and Loss of Function Resulting from Optical MCH Silencing during Warm Temperature Pulsing

(A) Protocol showing the three conditions, including constant T_a (baseline condition), MCH optical silencing (Opto Silen condition), or the combination of four bouts of warm T_a pulsing time locked with MCH silencing (Opto Silen+T condition).

(B) Four 30-min bouts of semi-chronic optical MCH silencing were performed bilaterally using a green laser (532 nm at 30 mW) in mice transduced with either ArchT or YFP.

(C) REM sleep expression significantly increased in the YFP group (n = 6; white) during T_a warming, an effect that appeared to be blocked in ArchT mice (n = 7; green).

(D–F) Percent change in total REM sleep duration with respect to the baseline condition during optical silencing alone or in combination with warm temperature pulsing for both 60-min bin (D) and 30-min bin (E and F) analyses.

(G) Photomicrographs show YFP expression (green), MCH neurons (red), and with overlay of double-fluorescence-labeled neurons (yellow). Scale bars: 100 μm.

Data were analyzed in (C) using repeated measures 2-way ANOVA and post-hoc Sidak's comparison test. Two-tailed Student's t tests were performed for (D)–(F). Data are means ± SEM. *p < 0.05; **p < 0.01; ***p < 0.001.

See also Figure S4.

latter data suggest that, although the MCH system is necessary for the dynamic increase in REM sleep expression during T_a warming, its silencing will not decrease REM sleep below baseline values. Finally, immunohistochemical analyses demonstrated 84% of MCH cells showing YFP staining and a high level of specificity with only 5% of YFP cells lacking immunoreactivity for MCH (Figure 4G).

DISCUSSION

We demonstrate for the first time a critical role for the MCH system in modulating REM sleep expression as a function of T_a. These data show that WT mice increase REM sleep during T_a warming but that MCHR1-KO mice show no significant changes in REM sleep as a function of T_a. The ability to increase

REM sleep during warm T_a pulsing was independent of T_b and specific to the light (inactive) circadian phase. This effect was specific to REM sleep in that rapid, or transient, T_a warming within the TNZ resulted in no significant changes to either NREM sleep or wakefulness. An increase in sleep pressure following 4 h of sleep deprivation was unable to rescue this temperature effect of REM sleep in mice lacking the MCHR1 receptor. Moreover, WT mice during recovery sleep demonstrated a dynamic ability to selectively increase REM sleep specifically during warm temperature pulsing.

In contrast to the loss of function seen in the MCHR1-KO mice, MCH optical activation for the first 30 min of the 60-min warming phases was able to overdrive the expression of REM sleep beyond what T_a warming alone was able to achieve. This increase in REM sleep in ChR2 mice was also noted during the last 15-min bin of the warming session following cessation of MCH stimulation, suggesting a prolonged effect from MCH activation on REM sleep expression. This prolonged effect, together with the loss of function observed in MCHR1-KO mice, would be consistent with the hypothesized role of the MCH neuropeptide, at least in part, mediating the REM sleep response. Finally, silencing of MCH neurons during T_a warming in ArchT mice was able to completely block the REM sleep response seen in YFP controls, confirming that the MCH system is necessary for the dynamic increase in REM sleep during T_a warming.

Ambient Temperature, Sleep, and the Role of the Hypothalamus

It is well established that sleep and thermoregulatory control are tightly integrated. This integration occurs in the anterior hypothalamus, which contains warm sensitive neurons intermingled with, or including, sleep active neurons responsible for NREM sleep generation [4, 18–20, 22]. For example, T_a warming to a static constant temperature of 32°C presented during the dark (active) phase in mice significantly increases NREM sleep while decreasing core body temperature with sleep initiation [19]. Through c-Fos-dependent activity tagging of neurons in the median preoptic (MnPO) and medial preoptic (MPO) anterior hypothalamic area, this work demonstrates that reactivation of these neurons can recapitulate sleep induction and the concomitant decrease in core body temperature. Moreover, the sleep-inducing effects of T_a warming are not caused by changes in core body temperature but likely mediated through skin thermosensors and their relay connections through the brainstem to these anterior hypothalamic structures [19].

Although NREM sleep may be modulated by T_a warming, REM sleep is actually more sensitive to T_a manipulation than NREM sleep [4, 16]. In our experiments, we restricted the T_a manipulation to a narrow range within the TNZ so that changes in REM sleep expression may occur without causing significant alterations in NREM sleep. In this manner, we were able to eliminate NREM sleep as a confounding variable driving changes in REM sleep expression. We found that mice generally responded to the warm T_a pulsing with an increase in REM sleep bout number. However, mice with increased sleep pressure, as seen in the second set of experiments, also showed a tendency to exhibit longer REM sleep bout durations. It is important to note that rodents sleeping in ambient temperatures below the TNZ preferentially reduce REM sleep over NREM sleep, demonstrating a shortening of REM sleep bout durations and a prolongation of REM-REM cycle lengths [16]. These latter data demonstrate the greater breadth of how endotherms might modulate REM sleep expression across a much wider T_a range. Taken together, these observations predict the presence of neural circuits responsible for REM sleep modulation as a function of T_a.

The MCH System and REM Sleep Control

The output control from the hypothalamus for REM sleep modulation during T_a warming has remained unknown. Our data suggest that the MCH system is necessary for the dynamic ability of the organism to opportunistically increase REM sleep when the need for core body temperature defense is minimized. Although the input modulation of the MCH system from anterior hypothalamic thermosensitive structures remains to be elucidated, we hypothesize that the MCH system, together with other structures within the posterior LH, plays a major role in integrating numerous biological variables for the output control of REM sleep [7]. In addition to ambient temperature as shown in Figure 5, these input variables may also include sleep pressure [35–38], energy status [39–41], and circadian time [42–44]. We speculate that these additional variables may also influence the receptivity of the organism to modulate REM sleep as a function of T_a.

The MCH system has been strongly implicated in the control of REM sleep, at least in part through GABAergic neurotransmission, given the known co-expression with glutamate decarboxylase 67 [45]. MCH neurons may mediate this effect through descending projections to brainstem REM-sleep-generating systems [46, 47]. Early work using REM sleep deprivation and c-Fos expression demonstrated that MCH neurons appear most active after a REM sleep rebound [28, 45]. Direct recordings of MCH neuronal activity demonstrate maximal firing during REM sleep and minimal activity during either NREM sleep or wakefulness, in contrast to hypocretin (Hcrt) neurons, which show a reciprocal activity pattern with greatest activity in wake [33, 34]. Optogenetic stimulation of MCH neurons during NREM sleep increases the number of transitions to REM sleep [23, 24], whereas the state-specific activation of MCH neurons during REM sleep prolongs REM bout durations [23]. Finally, chemogenetic activation of MCH neurons facilitates REM sleep onset and maintenance [26, 27]. Our findings using short duration (30-min) optogenetic activation of MCH neurons (semi-chronic and non-state specific) are consistent with these data. Specifically, we observed an increase in REM sleep arising primarily from an increase in the number of REM sleep bouts but with no significant effects on NREM sleep or wake durations.

Although MCH activation may promote REM sleep, effects of its inactivation or selective destruction are less clear. For example, optogenetic silencing of MCH neurons using either the eNpHR3.0 or ArchT opsin does not significantly reduce REM sleep durations below baseline [23, 24]. Moreover, selective chemogenetic inhibition, or destruction employing diphtheria toxin, show small alterations of the diurnal rhythm of wake and REM sleep without affecting their total durations [26, 48]. Finally, MCHR1-KO mice show no significant impact on REM sleep recovery following sleep deprivation compared to WT mice under constant T_a conditions [49]. Our results are also consistent with these previous findings. We show that MCH silencing failed to

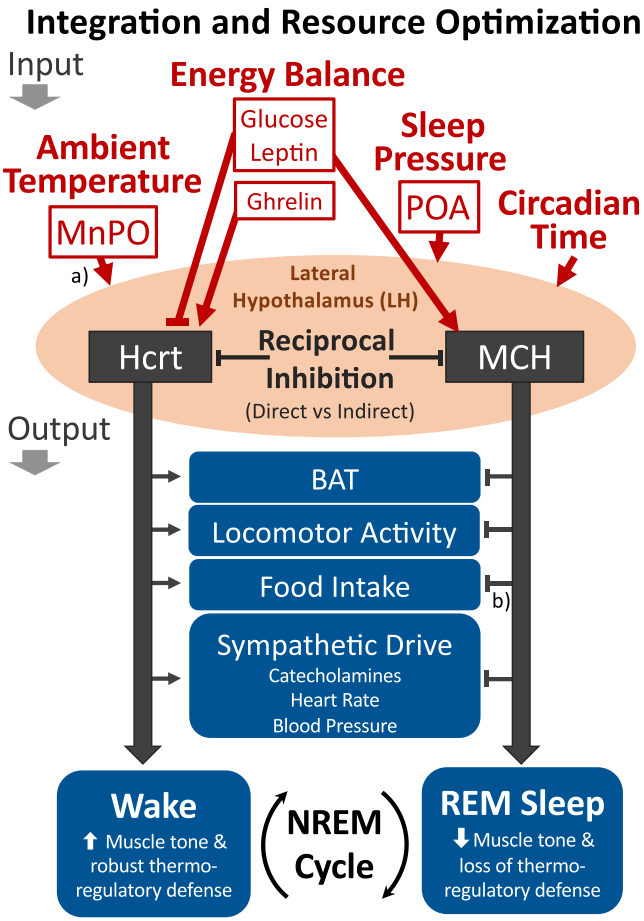

Figure 5. Proposed Role of MCH and the Lateral Hypothalamus (LH) to Promote Resource Optimization through the Cycling of NREM Sleep to Either Wakefulness or REM Sleep

The LH contains numerous cell types, including MCH and Hcrt neurons, which show a reciprocal firing pattern with MCH activity maximal in REM sleep and Hcrt activity maximal in wake [33]. These data suggest either direct or indirect reciprocal inhibition [34]. Numerous input variables may modulate the LH (see text). The MCH and Hcrt systems also exhibit opposing effects on many peripheral physiological processes. For example, whereas Hcrt promotes wakefulness, brown adipose tissue (BAT) activity, locomotion, food intake, and sympathetic drive, the MCH system promotes REM sleep and an inhibition of many of these same peripheral systems. We propose that several input variables, such as warm ambient temperature, positive energy balance, high sleep pressure, or the inactive circadian phase, may shift the balance toward the MCH system and REM sleep expression. An increased drive for REM sleep may manifest as a greater probability for NREM to REM sleep transitions, a decrease in inter-REM intervals, or an increase in REM sleep bout durations. (a) The MnPO and POA contain warm sensitive neurons that may directly or indirectly modulate the LH. (b) MCH may either increase or decrease food intake, depending on food availability and energy status. Straight arrowheads or bars represent activation or inhibition, respectively. MnPO, median preoptic nucleus; POA, preoptic area. Reprinted with permission from [7].

decrease REM sleep below baseline values and that REM sleep recovery was not altered following sleep deprivation compared to WT mice under constant conditions. However, we demonstrate that dynamic increases in REM sleep during T_a warming are abolished either following optogenetic silencing of MCH neurons or in mice lacking the MCHR1 receptor.

Taken together, our data suggest that, although MCH neurons play an important role driving the dynamic expression of REM sleep, neural structures other than MCH are necessary for decreasing REM sleep below baseline values. A potential candidate structure within the LH responsible for decreasing REM sleep is the Hcrt system [7, 50], at least in part through its direct and indirect reciprocal inhibition with MCH neurons [34]. Indeed, Hcrt may oppose REM sleep by not only decreasing MCH activity but also by concomitantly favoring waking systems.

We propose that the MCH system is part of a greater integrative circuit within the LH involving numerous neural structures, such as Hcrt for behavioral state output expression. Indeed, both Hcrt and MCH are also known to play important roles in energy balance in that they show opposite responsiveness patterns to biomarkers of hunger and satiety [7, 40, 41]. In this manner, conditions that favor Hcrt activity, such as negative energy balance, the active circadian phase, low sleep pressure, and cold ambient temperature, may potentially suppress REM sleep by decreasing MCH activity and driving waking systems (see Figure 5). However, conditions that favor MCH activity, such as positive energy balance, the inactive circadian phase, high sleep pressure, or a warm thermoneutral T_a, may shift the balance toward REM sleep expression via MCH activation and inhibition of Hcrt activity [7]. As an integrative circuit, it remains to be determined to what extent other cell types within the LH may also contribute toward REM sleep expression during T_a manipulation.

The EA Hypothesis: REM Sleep Expression and Ambient Temperature Integration

The EA hypothesis proposes that REM sleep is a behavioral strategy that promotes global shifts in whole-organism resource allocations away from costly thermoregulatory defenses toward REM-sleep-coupled biological functions [5, 7]. This theory suggests that many diverse biological processes are specifically upregulated during REM sleep to provide a selective advantage in subsequent wakefulness for maximization of reproductive success and evolutionary fitness [5]. These functions may include memory consolidation [51, 52], sensory-motor integration [53, 54], visual system development and maintenance [55–57], and reproductive function as seen by the appearance of penile erections in some mammals during REM sleep [58].

Endothermy, or maintaining a constant body temperature, increases energy expenditures approximately 10-fold over similar-sized poikilotherms when controlling for body mass [8, 9]. Importantly, REM sleep is characterized by a loss of thermoregulatory control [1, 3, 4] and a marked decrease in peripheral metabolic activity, as seen by the generalized skeletal muscle atonia in association with decreases in liver and brown adipose tissue (BAT) temperatures [59] and presumed BAT function [60]. In contrast, brain temperature and brain metabolic rate significantly increase during REM sleep [61–64].

These findings are consistent with a major internal reallocation of resources during REM sleep away from the periphery toward CNS-related processes [5]. The brain and reproduction function are viewed as major beneficiaries of this energy allocation strategy of REM sleep. Whole-organism metabolic rate demonstrates minimal alterations when comparing NREM with REM sleep [65–67]. By shifting resource allocations away from the periphery

into the CNS, REM sleep is viewed by the EA hypothesis as a net-energy neutral state compared to NREM sleep.

The presence of neural circuits that drive REM sleep expression when the need for thermoregulatory defense is minimized advocates a whole-organism perspective of resource optimization [5, 7]. An alternative evolutionary strategy would be to upregulate REM-related functions irrespective of T_a while maintaining thermoregulatory defense. This latter strategy would theoretically constrain available resources for such investments if total energy expenditure is to remain stable or otherwise increase total energy requirements.

The EA hypothesis postulates that evolutionary selective pressures have driven species-specific REM sleep bout durations and NREM-REM sleep cycle lengths in response to thermoregulatory constraints [5, 7]. Prolonged REM sleep bout durations, for example, are more likely associated with core body temperature deviations toward the ambient temperature [68, 69]. REM sleep bout durations are thus constrained by the organism's surface-area-to-volume ratio and its ability to retain heat [5, 7]. By constraining REM sleep bout durations, as well as by cycling REM sleep with NREM sleep, organisms may theoretically minimize energy expenditures defending the core temperature while maximizing REM sleep expression.

The EA hypothesis of REM sleep is consistent with the strong positive correlation between REM-REM cycle length and body mass across mammalian species [70]. Small species with large surface-area-to-volume ratios, such as the mouse, for example, have particularly short REM sleep bout durations and either cycle rapidly from one REM bout to the next or show intervening wakefulness. However, the slope of this positive correlation between body mass and cycle length is considerably lower than what would be expected if this relationship were simply based on metabolic rate [5]. We hypothesize that REM sleep bout durations should also positively correlate with body mass across species and that other variables, such as fat stores, thickness of fur, and the ambient temperature of the environment, may further contribute to REM sleep bout duration and cycle length optimization.

The ability to modulate REM sleep as a function of T_a has important evolutionary implications. Specifically, organisms that optimize competing investments related to thermoregulation versus CNS-related plasticity, growth, and development may thus maximize efficiencies in managing energy constraints. To illustrate, the ontogenetic hypothesis suggests that altricial species born with a comparatively small brain compared to adulthood exhibit markedly elevated REM sleep quantities at birth to promote rapid brain development [55]. It is noteworthy that the effects of T_a warming on triggering REM sleep are particularly pronounced in neonates. For example, REM sleep in neonatal rat pups is maximally expressed as the T_a approaches ~35°C, whereas it is significantly decreased as the T_a falls below 27°C and may be suspended entirely when the T_a is decreased below 23°C [71, 72].

In the wild, T_a varies considerably across circadian time and season. By opportunistically harnessing heat generated from the environment or from a nest microclimate, the EA hypothesis proposes that endotherms, such as mice, are able to defer costs of individual thermoregulation during REM sleep and direct available resources, instead, into CNS-related processes. Our data suggest that the MCH system is critical to increase REM sleep when in thermoneutral, ambient temperatures. More data are required to elucidate neural mechanisms responsible for reducing REM sleep to favor thermoregulatory defenses associated with wakefulness or NREM sleep when T_a deviates from thermoneutrality. In a broader perspective, we propose that the MCH system is part of a larger integrative circuit within the LH. The ability of the LH to also integrate energy status, sleep pressure, and circadian time for behavioral state expression places the MCH system in a key position to regulate global shifts in resource allocations central to the EA hypothesis of sleep function.

STAR★METHODS

Detailed methods are provided in the online version of this paper and include the following:

- KEY RESOURCES TABLE
- CONTACT FOR REAGENT AND RESOURCE SHARING
- EXPERIMENTAL MODEL AND SUBJECT DETAILS
  - Mice
- METHOD DETAILS
  - Plasmid construction and rAAV packaging
  - Surgical procedures
  - Electrophysiological recordings
  - Optical illumination protocol
  - Ambient temperature manipulation protocol
  - Sleep deprivation
  - Offline polysomnographic data analysis
  - EEG Power Spectrum
  - Immunohistochemical labeling
- QUANTIFICATION AND STATISTICAL ANALYSIS
  - Statistical Analyses
- DATA AND SOFTWARE AVAILABILITY

SUPPLEMENTAL INFORMATION

Supplemental Information can be found online at https://doi.org/10.1016/j.cub.2019.05.009.

ACKNOWLEDGMENTS

We would like to thank Mary Gazea, Carlos Del Rio-Bermudez, Lisa Branca, and Dorothee Hausmann for their specific contributions toward data analyses. We would also like to thank members of the ZEN laboratory for their technical assistance. This work is supported by the Center for Experimental Neurology and the Department of Neurology at the University of Bern, Bern University Hospital (Inselspital), as well as the Insel grant 84801184, the Sleep Medicine Research Foundation, and the Ohio Sleep Medicine Institute. A.A. was supported by the Human Frontier Science Program (RGY0076/2012), Inselspital University Hospital Bern, Swiss National Science Foundation (31003A_156156), European Research Council (725850), Sinergia (CRSII3_160803), and the University of Bern.

AUTHOR CONTRIBUTIONS

N.K., B.L., and M.H.S. performed experiments, analyzed data, performed statistical analyses, and generated figures. T.R. wrote code for MATLAB and performed computational analyses of brain temperature recordings. M.H.S. and A.A. designed the experiments. All authors contributed to manuscript revisions. M.H.S. wrote the manuscript with contributions from N.K. M.H.S. conceived the project and directly supervised the work.

DECLARATION OF INTERESTS

The authors declare no competing interests.

Received: February 14, 2019
Revised: April 2, 2019
Accepted: May 1, 2019
Published: May 30, 2019

REFERENCES

1. Parmeggiani, P.L. (2003). Thermoregulation and sleep. Front. Biosci. *8*, s557–s567.
2. Schmidek, W.R., Zachariassen, K.E., and Hammel, H.T. (1983). Total calorimetric measurements in the rat: influences of the sleep-wakefulness cycle and of the environmental temperature. Brain Res. *288*, 261–271.
3. Heller, H.C. (2005). Temperature thermoregulation and sleep. In Principles and Practice of Sleep Medicine, Fourth Edition, M. Kryger, T. Roth, and W. Dement, eds. (Elsivier Saunders).
4. Cerri, M., Luppi, M., Tupone, D., Zamboni, G., and Amici, R. (2017). REM sleep and endothermy: potential sites and mechanism of a reciprocal interference. Front. Physiol. *8*, 624.
5. Schmidt, M.H. (2014). The energy allocation function of sleep: a unifying theory of sleep, torpor, and continuous wakefulness. Neurosci. Biobehav. Rev. *47*, 122–153.
6. Schmidt, M.H., Swang, T.W., Hamilton, I.M., and Best, J.A. (2017). State-dependent metabolic partitioning and energy conservation: a theoretical framework for understanding the function of sleep. PLoS ONE *12*, e0185746.
7. Latifi, B., Adamantidis, A., Bassetti, C., and Schmidt, M.H. (2018). Sleep-wake cycling and energy conservation: role of hypocretin and the lateral hypothalamus in dynamic state-dependent resource optimization. Front. Neurol. *9*, 790.
8. Hulbert, A.J., and Else, P.L. (1989). Evolution of mammalian endothermic metabolism: mitochondrial activity and cell composition. Am. J. Physiol. *256*, R63–R69.
9. Körtner, G., and Geiser, F. (2000). The temporal organization of daily torpor and hibernation: circadian and circannual rhythms. Chronobiol. Int. *17*, 103–128.
10. Szymusiak, R., and Satinoff, E. (1981). Maximal REM sleep time defines a narrower thermoneutral zone than does minimal metabolic rate. Physiol. Behav. *26*, 687–690.
11. Szymusiak, R., Satinoff, E., Schallert, T., and Whishaw, I.Q. (1980). Brief skin temperature changes towards thermoneutrality trigger REM sleep in rats. Physiol. Behav. *25*, 305–311.
12. Muzet, A., Libert, J.P., and Candas, V. (1984). Ambient temperature and human sleep. Experientia *40*, 425–429.
13. Kumar, D., Mallick, H.N., and Kumar, V.M. (2009). Ambient temperature that induces maximum sleep in rats. Physiol. Behav. *98*, 186–191.
14. Muzet, A., Ehrhart, J., Candas, V., Libert, J.P., and Vogt, J.J. (1983). REM sleep and ambient temperature in man. Int. J. Neurosci. *18*, 117–126.
15. Amici, R., Cerri, M., Ocampo-Garcés, A., Baracchi, F., Dentico, D., Jones, C.A., Luppi, M., Perez, E., Parmeggiani, P.L., and Zamboni, G. (2008). Cold exposure and sleep in the rat: REM sleep homeostasis and body size. Sleep *31*, 708–715.
16. Cerri, M., Ocampo-Garces, A., Amici, R., Baracchi, F., Capitani, P., Jones, C.A., Luppi, M., Perez, E., Parmeggiani, P.L., and Zamboni, G. (2005). Cold exposure and sleep in the rat: effects on sleep architecture and the electroencephalogram. Sleep *28*, 694–705.
17. Alam, M.N., McGinty, D., and Szymusiak, R. (1995). Neuronal discharge of preoptic/anterior hypothalamic thermosensitive neurons: relation to NREM sleep. Am. J. Physiol. *269*, R1240–R1249.
18. Tan, C.L., Cooke, E.K., Leib, D.E., Lin, Y.-C., Daly, G.E., Zimmerman, C.A., and Knight, Z.A. (2016). Warm-sensitive neurons that control body temperature. Cell *167*, 47–59.e15.
19. Harding, E.C., Yu, X., Miao, A., Andrews, N., Ma, Y., Ye, Z., Lignos, L., Miracca, G., Ba, W., Yustos, R., et al. (2018). A neuronal hub binding sleep initiation and body cooling in response to a warm external stimulus. Curr. Biol. *28*, 2263–2273.e4.
20. Szymusiak, R. (2018). Body temperature and sleep. Handb. Clin. Neurol. *156*, 341–351.
21. Szymusiak, R., Gvilia, I., and McGinty, D. (2007). Hypothalamic control of sleep. Sleep Med. *8*, 291–301.
22. Kroeger, D., Absi, G., Gagliardi, C., Bandaru, S.S., Madara, J.C., Ferrari, L.L., Arrigoni, E., Münzberg, H., Scammell, T.E., Saper, C.B., and Vetrivelan, R. (2018). Galanin neurons in the ventrolateral preoptic area promote sleep and heat loss in mice. Nat. Commun. *9*, 4129.
23. Jego, S., Glasgow, S.D., Herrera, C.G., Ekstrand, M., Reed, S.J., Boyce, R., Friedman, J., Burdakov, D., and Adamantidis, A.R. (2013). Optogenetic identification of a rapid eye movement sleep modulatory circuit in the hypothalamus. Nat. Neurosci. *16*, 1637–1643.
24. Tsunematsu, T., Ueno, T., Tabuchi, S., Inutsuka, A., Tanaka, K.F., Hasuwa, H., Kilduff, T.S., Terao, A., and Yamanaka, A. (2014). Optogenetic manipulation of activity and temporally controlled cell-specific ablation reveal a role for MCH neurons in sleep/wake regulation. J. Neurosci. *34*, 6896–6909.
25. Blanco-Centurion, C., Liu, M., Konadhode, R.P., Zhang, X., Pelluru, D., van den Pol, A.N., and Shiromani, P.J. (2016). Optogenetic activation of melanin-concentrating hormone neurons increases non-rapid eye movement and rapid eye movement sleep during the night in rats. Eur. J. Neurosci. *44*, 2846–2857.
26. Vetrivelan, R., Kong, D., Ferrari, L.L., Arrigoni, E., Madara, J.C., Bandaru, S.S., Lowell, B.B., Lu, J., and Saper, C.B. (2016). Melanin-concentrating hormone neurons specifically promote rapid eye movement sleep in mice. Neuroscience *336*, 102–113.
27. Varin, C., Luppi, P.-H., and Fort, P. (2018). Melanin-concentrating hormone-expressing neurons adjust slow-wave sleep dynamics to catalyze paradoxical (REM) sleep. Sleep (Basel) *41*, zsy068.
28. Verret, L., Goutagny, R., Fort, P., Cagnon, L., Salvert, D., Léger, L., Boissard, R., Salin, P., Peyron, C., and Luppi, P.-H. (2003). A role of melanin-concentrating hormone producing neurons in the central regulation of paradoxical sleep. BMC Neurosci. *4*, 19.
29. Peyron, C., Sapin, E., Leger, L., Luppi, P.-H., and Fort, P. (2009). Role of the melanin-concentrating hormone neuropeptide in sleep regulation. Peptides *30*, 2052–2059.
30. Monti, J.M., Torterolo, P., and Lagos, P. (2013). Melanin-concentrating hormone control of sleep-wake behavior. Sleep Med. Rev. *17*, 293–298.
31. Gordon, C.J. (2012). Thermal physiology of laboratory mice: defining thermoneutrality. J. Therm. Biol. *37*, 654–685.
32. Gordon, C.J., Becker, P., and Ali, J.S. (1998). Behavioral thermoregulatory responses of single- and group-housed mice. Physiol. Behav. *65*, 255–262.
33. Hassani, O.K., Lee, M.G., and Jones, B.E. (2009). Melanin-concentrating hormone neurons discharge in a reciprocal manner to orexin neurons across the sleep-wake cycle. Proc. Natl. Acad. Sci. USA *106*, 2418–2422.
34. Apergis-Schoute, J., Iordanidou, P., Faure, C., Jego, S., Schöne, C., Aitta-Aho, T., Adamantidis, A., and Burdakov, D. (2015). Optogenetic evidence for inhibitory signaling from orexin to MCH neurons via local microcircuits. J. Neurosci. *35*, 5435–5441.
35. Rao, Y., Liu, Z.-W., Borok, E., Rabenstein, R.L., Shanabrough, M., Lu, M., Picciotto, M.R., Horvath, T.L., and Gao, X.-B. (2007). Prolonged wakefulness induces experience-dependent synaptic plasticity in mouse hypocretin/orexin neurons. J. Clin. Invest. *117*, 4022–4033.
36. Rai, S., Kumar, S., Alam, M.A., Szymusiak, R., McGinty, D., and Alam, M.N. (2010). A1 receptor mediated adenosinergic regulation of

perifornical-lateral hypothalamic area neurons in freely behaving rats. Neuroscience *167*, 40–48.

37. Saper, C.B., Chou, T.C., and Scammell, T.E. (2001). The sleep switch: hypothalamic control of sleep and wakefulness. Trends Neurosci. *24*, 726–731.
38. Toossi, H., Del Cid-Pellitero, E., and Jones, B.E. (2016). GABA receptors on orexin and melanin-concentrating hormone neurons are differentially homeostatically regulated following sleep deprivation. eNeuro *3*, ENEURO.0077-16.2016.
39. Louis, G.W., Leinninger, G.M., Rhodes, C.J., and Myers, M.G., Jr. (2010). Direct innervation and modulation of orexin neurons by lateral hypothalamic LepRb neurons. J. Neurosci. *30*, 11278–11287.
40. Yamanaka, A., Beuckmann, C.T., Willie, J.T., Hara, J., Tsujino, N., Mieda, M., Tominaga, M., Yagami, Ki., Sugiyama, F., Goto, K., et al. (2003). Hypothalamic orexin neurons regulate arousal according to energy balance in mice. Neuron *38*, 701–713.
41. Burdakov, D., Gerasimenko, O., and Verkhratsky, A. (2005). Physiological changes in glucose differentially modulate the excitability of hypothalamic melanin-concentrating hormone and orexin neurons in situ. J. Neurosci. *25*, 2429–2433.
42. Marston, O.J., Williams, R.H., Canal, M.M., Samuels, R.E., Upton, N., and Piggins, H.D. (2008). Circadian and dark-pulse activation of orexin/hypocretin neurons. Mol. Brain *1*, 19.
43. Tyree, S.M., Borniger, J.C., and de Lecea, L. (2018). Hypocretin as a hub for arousal and motivation. Front. Neurol. *9*, 413.
44. Appelbaum, L., Wang, G., Yokogawa, T., Skariah, G.M., Smith, S.J., Mourrain, P., and Mignot, E. (2010). Circadian and homeostatic regulation of structural synaptic plasticity in hypocretin neurons. Neuron *68*, 87–98.
45. Sapin, E., Bérod, A., Léger, L., Herman, P.A., Luppi, P.-H., and Peyron, C. (2010). A very large number of GABAergic neurons are activated in the tuberal hypothalamus during paradoxical (REM) sleep hypersomnia. PLoS ONE *5*, e11766.
46. Clément, O., Sapin, E., Libourel, P.-A., Arthaud, S., Brischoux, F., Fort, P., and Luppi, P.-H. (2012). The lateral hypothalamic area controls paradoxical (REM) sleep by means of descending projections to brainstem GABAergic neurons. J. Neurosci. *32*, 16763–16774.
47. Kroeger, D., Bandaru, S.S., Madara, J.C., and Vetrivelan, R. (2019). Ventrolateral periaqueductal gray mediates rapid eye movement sleep regulation by melanin-concentrating hormone neurons. Neuroscience *406*, 314–324.
48. Varin, C., Arthaud, S., Salvert, D., Gay, N., Libourel, P.-A., Luppi, P.-H., Léger, L., and Fort, P. (2016). Sleep architecture and homeostasis in mice with partial ablation of melanin-concentrating hormone neurons. Behav. Brain Res. *298* (Pt B), 100–110.
49. Adamantidis, A., Salvert, D., Goutagny, R., Lakaye, B., Gervasoni, D., Grisar, T., Luppi, P.-H., and Fort, P. (2008). Sleep architecture of the melanin-concentrating hormone receptor 1-knockout mice. Eur. J. Neurosci. *27*, 1793–1800.
50. Roman, A., Meftah, S., Arthaud, S., Luppi, P.-H., and Peyron, C. (2018). The inappropriate occurrence of rapid eye movement sleep in narcolepsy is not due to a defect in homeostatic regulation of rapid eye movement sleep. Sleep (Basel) *41*, zsy046.
51. Boyce, R., Williams, S., and Adamantidis, A. (2017). REM sleep and memory. Curr. Opin. Neurobiol. *44*, 167–177.
52. Boyce, R., Glasgow, S.D., Williams, S., and Adamantidis, A. (2016). Causal evidence for the role of REM sleep theta rhythm in contextual memory consolidation. Science *352*, 812–816.
53. Blumberg, M.S. (2015). Developing sensorimotor systems in our sleep. Curr. Dir. Psychol. Sci. *24*, 32–37.
54. Del Rio-Bermudez, C., and Blumberg, M.S. (2018). Active sleep promotes functional connectivity in developing sensorimotor networks. BioEssays *40*, e1700234.
55. Roffwarg, H.P., Muzio, J.N., and Dement, W.C. (1966). Ontogenetic development of the human sleep-dream cycle. Science *152*, 604–619.
56. Frank, M.G. (2015). Sleep and synaptic plasticity in the developing and adult brain. Curr. Top. Behav. Neurosci. *25*, 123–149.
57. Dumoulin Bridi, M.C., Aton, S.J., Seibt, J., Renouard, L., Coleman, T., and Frank, M.G. (2015). Rapid eye movement sleep promotes cortical plasticity in the developing brain. Sci. Adv. *1*, e1500105.
58. Schmidt, M.H., Valatx, J.L., Sakai, K., Fort, P., and Jouvet, M. (2000). Role of the lateral preoptic area in sleep-related erectile mechanisms and sleep generation in the rat. J. Neurosci. *20*, 6640–6647.
59. Dewasmes, G., Loos, N., Delanaud, S., Ramadan, W., and Dewasmes, D. (2003). Liver temperature during sleep. Sleep *26*, 948–950.
60. Calasso, M., Zantedeschi, E., and Parmeggiani, P.L. (1993). Cold-defense function of brown adipose tissue during sleep. Am. J. Physiol. *265*, R1060–R1064.
61. Madsen, P.L., Schmidt, J.F., Wildschiødtz, G., Friberg, L., Holm, S., Vorstrup, S., and Lassen, N.A. (1991). Cerebral O2 metabolism and cerebral blood flow in humans during deep and rapid-eye-movement sleep. J. Appl. Physiol. *70*, 2597–2601.
62. Silvani, A., Asti, V., Berteotti, C., Bojic, T., Cianci, T., Ferrari, V., Franzini, C., Lenzi, P., and Zoccoli, G. (2005). Sleep-related brain activation does not increase the permeability of the blood-brain barrier to glucose. J. Cereb. Blood Flow Metab. *25*, 990–997.
63. Madsen, P.L., and Vorstrup, S. (1991). Cerebral blood flow and metabolism during sleep. Cerebrovasc. Brain Metab. Rev. *3*, 281–296.
64. Maquet, P., Dive, D., Salmon, E., Sadzot, B., Franco, G., Poirrier, R., von Frenckell, R., and Franck, G. (1990). Cerebral glucose utilization during sleep-wake cycle in man determined by positron emission tomography and [18F]2-fluoro-2-deoxy-D-glucose method. Brain Res. *513*, 136–143.
65. Jung, C.M., Melanson, E.L., Frydendall, E.J., Perreault, L., Eckel, R.H., and Wright, K.P. (2011). Energy expenditure during sleep, sleep deprivation and sleep following sleep deprivation in adult humans. J. Physiol. *589*, 235–244.
66. Zhang, S., Zeitzer, J.M., Sakurai, T., Nishino, S., and Mignot, E. (2007). Sleep/wake fragmentation disrupts metabolism in a mouse model of narcolepsy. J. Physiol. *581*, 649–663.
67. Katayose, Y., Tasaki, M., Ogata, H., Nakata, Y., Tokuyama, K., and Satoh, M. (2009). Metabolic rate and fuel utilization during sleep assessed by whole-body indirect calorimetry. Metabolism *58*, 920–926.
68. Walker, J.M., Walker, L.E., Harris, D.V., and Berger, R.J. (1983). Cessation of thermoregulation during REM sleep in the pocket mouse. Am. J. Physiol. *244*, R114–R118.
69. Sichieri, R., and Schmidek, W.R. (1984). Influence of ambient temperature on the sleep-wakefulness cycle in the golden hamster. Physiol. Behav. *33*, 871–877.
70. Savage, V.M., and West, G.B. (2007). A quantitative, theoretical framework for understanding mammalian sleep. Proc. Natl. Acad. Sci. USA *104*, 1051–1056.
71. Blumberg, M.S., and Stolba, M.A. (1996). Thermogenesis, myoclonic twitching, and ultrasonic vocalization in neonatal rats during moderate and extreme cold exposure. Behav. Neurosci. *110*, 305–314.
72. Seelke, A.M.H., and Blumberg, M.S. (2005). Thermal and nutritional modulation of sleep in infant rats. Behav. Neurosci. *119*, 603–611.
73. Adamantidis, A., Thomas, E., Foidart, A., Tyhon, A., Coumans, B., Minet, A., Tirelli, E., Seutin, V., Grisar, T., and Lakaye, B. (2005). Disrupting the melanin-concentrating hormone receptor 1 in mice leads to cognitive deficits and alterations of NMDA receptor function. Eur. J. Neurosci. *21*, 2837–2844.

STAR★METHODS

KEY RESOURCES TABLE

REAGENT or RESOURCE	SOURCE	IDENTIFIER
Antibodies		
Rabbit anti-GFP (Rb pAB to GFP)	Abcam	Cat# ab290; RRID: AB_303395
Goat anti-MCH (pro-MCH (C-20) goat polyclonal IgG)	Santa Cruz	Cat# sc-14509; RRID: AB_2237276
Donkey anti-rabbit (Donkey anti-Rabbit IgG (H+L))	Life Technologies	Cat# A-21206; RRID: AB_2535792
Donkey anti-goat (Donkey anti-Goat IgG (H+L))	Life Technologies	Cat# A-21432; RRID: AB_2535853
Bacterial and Virus Strains		
AAV2-EF1α-DIO-hChR2(H134R)-eYFP	University of North Carolina (USA)	AV4378L
AAV2-EF1α-DIO-ArchT3.0-eYFP	University of North Carolina (USA)	AV4881D
AAV2-EF1α-DIO-eYFP	University of North Carolina (USA)	AV4842d
Chemicals, Peptides, and Recombinant Proteins		
Forene (Isoflurane)	Abbvie	B5062
Metacam	Boehringer Ingelheim	10-138348
Cresyl violet Kluwer Barrera, staining solution	Labforce	05-B16001
Formaldehyde 4% buffered	Dr. Grogg Chemie AG	G256.1000
Phosphate-buffered saline, premix PBS-buffer 10x	Sigma-Aldrich Chemie GmbH	11666789001
Sucrose	VWR International AG	1.07687.1000
Methyl butane	Sigma-Aldrich Chemie GmbH	320404-1L
Fluoromount Aqueous Mounting Medium	Sigma-Aldrich Chemie GmbH	F4680-25ML
Experimental Models: Organisms/Strains		
Mouse: MCHR1 KO, MCHR1 tm1.1 Blak	Generated in our laboratory [73]	Cat# 3783583, RRID: MGI:3783583
Mouse: MCH-cre, tg(Pmch-cre)1Lowl/J	Bradford Lowell Laboratory	Cat# JAX:014099, RRID: IMSR_JAX:014099
Software and Algorithms		
SleepSign	Kissei Comtec, Matsumoto, Japan	http://www.sleepsign.com/
MATLAB	MathWorks	RRID: SCR_001622
GraphPad Prism version 7.04	GraphPad Software Inc, USA	RRID: SCR_002798
Spike2	Cambridge Electronic Design	RRID: SCR_000903
Other		
Stereotaxic apparatus	David Kopf Instruments	http://kopfinstruments.com/
Superbond C&B Catalyst	Prestige Dental Products Limited	7110
Superbond C&B Polymer	Prestige Dental Products Limited	7112-350
Superbond Quick Monomer	Prestige Dental Products Limited	7111-100
Paladur liquid, 500ml	Kaladent AG	64707938
Paladur powder, 100 g	Kaladent AG	64707948
Micro-BetaCHIP thermistor probe (MCD)	Measurement Specialties	https://www.te.com/usa-en/products/brands/meas.html?tab=pgp-story
Grass P122 AC/DC strain gage amplifier	Artisan Technology Group	https://www.artisantg.com/TestMeasurement/91397/Astro_Med_Grass_Technologies_P122_Series_AC_DC_Strain_Gage_Amplifiers
Diode laser	LaserGlow	https://www.laserglow.com/product/byproduct/TEM00-Diode-Lasers/
Master-9	Agilent technologies	https://www.agilent.com/
Cryostat	Leica Microsystems Hyrax C25,	51039
Glass slides, Superfrost Plus	VWR International AG	J1800AMNZ
Fluorescence microscope	Olympus	Model: Olympus BX 51 epifluorescence microscope

CONTACT FOR REAGENT AND RESOURCE SHARING

Further information and requests for resources and reagents should be directed to and will be fulfilled by the Lead Contact, Markus H. Schmidt (markus.schmidt@insel.ch).

EXPERIMENTAL MODEL AND SUBJECT DETAILS

Mice

Two genetically-modified mouse lines were used for these experiments, including MCH receptor-1 knock out mice (MCHR1-KO, also known to as MCHR1 tm1.1 Blak [73]) and mice expressing cre recombinase under the pro-MCH gene promotor (MCH-cre mice, tg(Pmch-cre)1Lowl/J). Homozygous MCHR1-KO (n = 11, MCHR1$^{-/-}$) and WT (n = 8, MCHR1$^{+/+}$) male mice were used for these experiments and maintained as previously described [49]. Heterozygous MCH-cre mice were maintained on a C57BL/6 genetic background by intercross breeding as previously described [23]. MCH-cre males (n = 27) were used for sleep recordings involving optogenetic experiments, including for the ChR2 group (n = 7), ArchT group (n = 7), and the YFP control groups (n = 13). The genotyping for all mice was verified using PCR from ear clip biopsies. Mice were aged between 10-20 weeks.

Experiments were performed at the laboratory Zentrum für Experimentelle Neurologie (ZEN) at the University Hospital, Inselspital, in Bern, Switzerland. All the experiments were carried out in accordance with the guidelines described in the National Institutes of Health Guide for the Care and Use of Laboratory Animals and the Bern Kanton Animal Care Committee.

METHOD DETAILS

Plasmid construction and rAAV packaging

For optogenetic experiments, we used adeno-associated virus (AAV) viruses encompassing genes for channelrhodopsin (AAV2-EF1α-DIO-hChR2(H134R)-eYFP), or the proton pump archaerhodopsin-T (AAV2-EF1α-DIO-ArchT3.0-eYFP). Control mice were injected with AAV2-EF1α-DIO-eYFP. The plasmids were packaged in AAV 2 serotype by the viral vector core facility at the University of North Carolina (USA).

Surgical procedures

Animals were anesthetized with isoflurane (2% in O2) and injected with (Metacam 0.1ml/kg s.c.) for analgesia. For optogenetic experiments as previously published [23], virus injections were performed on stereotactic frames, infused bilaterally in the LH of MCH-cre knock-in mice (AP: −1.5 mm, ML: ± 0.9 mm; DV: −5.35 mm) with 0.8 μL of high-titer AAV (> 10^{12} pfu/mL) at a rate of 0.1 μl/min using an 29-gauge internal cannula. After surgery, mice were single housed for recovery and AAV expression for at least 20 days.

One to two weeks following the virus injections, homemade bilateral optic fiber implants were then implanted above the LH (the coordinates of AP: −1.4 mm, ML: ± 0.95 mm; DV: −4.6 mm) and fixed to the skull with C&B Metabond (Patterson dental) and dental cement (Patterson dental) as previously described [23]. Electroencephalography (EEG) for all experiments was recorded from pairs of cortical electrode screws placed over the frontal and parietal cortices. Three wire electrodes were inserted in the dorsal neck musculature to record postural tone through electromyographic (EMG) activity. Electrodes were pre-soldered to a miniconnector cemented to the skull with C&B Metabond (Patterson dental) and dental cement (Patterson dental).

Brain temperature recordings were performed in WT mice (n = 4) using a Micro-BetaCHIP thermistor probe (MCD) from Measurement Specialties with outside diameter of 500 μm. Temperature probes were calibrated prior to implantation using water baths at three different temperatures and using a Grass P122 AC/DC strain gage amplifier. Temperature probes were implanted unilaterally into the rostral anterior hypothalamus of four mice (coordinates AP: +0.38 mm, ML: −1.2 mm, DV: −5.5 mm). Placement of the temperature probes were confirmed using cresyl violet staining.

Electrophysiological recordings

After recovery (10 days, single housed), mice were connected to flexible cables and, for optogenetic experiments, optical fibers for an additional 7-10 days of habituation to the recording conditions. Physiological signals were amplified (Grass Instruments) and digitized at 512 Hz using SleepSign® (Kissei Comtec, Matsumoto, Japan). Habituation was confirmed by verifying 24 h of baseline sleep-wake cycling.

Optical illumination protocol

Bilateral 200-μm optical fiber implants were coupled to a 473 nm (blue light) or 532 nm (green light) diode laser (LaserGlow) to deliver light into the brain at ~30 mW, as described in published reports [23]. Semi-chronic and state-independent optical stimulations were generated using wave-form generators (Master-9, Agilent technologies). Mice were exposed to the optical illumination protocol on two separate recording days at both constant temperature and again during the T_a manipulation protocol (see below) with at least 48 hours between illumination sessions. The protocol for the semi-chronic optogenetic stimulations using the blue laser (473 nm) involved 50 ms pulses at 20 Hz for 10 s stimulation-on and 20 s stimulation-off, repeated for 30 minutes (Figure 3B). The protocol for the optical silencing experiments using the green laser (532 nm) involved continuous illumination for 15 s-on and 15 s-off, repeated

for 30 minutes (Figure 4B). Optical illuminations were delivered at ZT 2, 4, 6, and 8 h. Placement of the optical fibers were verified for each animal after the experiment.

Ambient temperature manipulation protocol

A temperature-controlled cabinet was sized to fit 4 plexiglass cages to record 4 mice simultaneously during experiments, allowing for 2 experimental mice and 2 control mice during experimental sessions. The interior of the cabinet was lined with reflective aluminum tape and electrically grounded to create a Faraday cage. Two infrared (IR) lamps were positioned in a symmetrical fashion so that two pairs of cages were of equal distance from an IR heat source. The IR lamps were directed toward the ceiling of the cabinet to allow for a diffuse reflection of IR light for the rapid warming sessions. A convection heat source connected to a low pressure forced air circulation system was also used for warming of the cabinet. The IR lamps and the convection heat source were under thermostatic control using a programable timer for precise delivery of temperature manipulation.

Experimental mice were housed in individual plexiglass recording cages at constant ambient temperature (23 ± 1°C) and humidity (40%–60%) under a 12h/12h light/dark cycle (lights on at 7:00 am, or zeitgeber time 0). Food and water were available *ad libitum*. After another week of habituation, baseline recordings were performed, followed by a 3–5 day habituation to an ambient temperature (T_a) manipulation protocol.

The temperature manipulation protocol involved four bouts of rapid T_a warming to a maximum temperature of 32.0°C achieved over a period of approximately 15 min and with active warming terminated 30 min after bout initiation (Figure 1B). The four bouts of warm T_a pulsing were performed at two-hour intervals during the middle of the light period (ZT: 2, 4, 6, and 8). For experiments employing the T_a manipulation protocol during the circadian dark phase, the four bouts of warm temperature pulsing were administered in the middle of the dark period (ZT: 14, 16, 18, and 20). The active warming phase occurred over the first 30 min of the warming sessions, followed by passive cooling phases over the next 90 min. Ambient temperatures during the warming phases ranged between 27.5-32°C, producing four 60-min bins during which the T_a was at the high end of the mouse thermoneutral zone (TNZ warm condition). During passive cooling, the four TNZ warm periods were followed by four 60-min bins where the temperatures decreased below 27.5°C to approximately 24.5 C for an average temperature of approximately 25.6°C (TNZ cool condition).

Sleep deprivation

WT (n = 8) and MCHR1-KO mice (n = 6) underwent a 4-hr total sleep deprivation using gentle handling at the beginning of the light period (ZT 0-4 hr) during constant temperature (23.0 ± 1.0°C). EEG and EMG recordings were performed during sleep deprivation to confirm wakefulness during any periods of inactivity. Immediately following this protocol, the doors of the temperature-controlled cabinet were closed at ZT 4 h and the animals were then allowed to recover sleep. All mice underwent the sleep deprivation procedure twice with at least one week between sessions, but recovery sleep was performed using two different T_a conditions. Specifically, mice were allowed to recover sleep during either the constant T_a condition or during exposure to warm T_a pulsing as performed in prior experiments occurring at 2-h intervals. Recovery sleep with warm T_a pulsing thus involved three warming bouts at ZT 4, 6, and 8 h (Figure 2A). Mice undergoing temperature manipulation during the recovery period were habituated to the T_a manipulation protocol 3-5 days prior to the sleep deprivation experiment.

Offline polysomnographic data analysis

Polysomnographic recordings were visually scored by two independent scorers using SleepSign software using 5 s epochs. Scoring of wake, NREM and REM sleep involved analyses of EEG and EMG recordings. Wake was characterized by a low amplitude, mixed frequency EEG signal in association with a relatively elevated and variable EMG muscle tone and activity. NREM sleep was defined by EEG showing synchronous high amplitude slow wave activity in the delta frequency range (0.5-4 Hz) with a low and stable muscle tone. Finally, REM sleep was characterized by theta oscillations (6-9 Hz) and a neck muscle atonia. Power spectral data from 5 s epochs were simultaneously displayed during manual scoring. Transitions to and from NREM or REM sleep were scored based on peak power in the delta or theta bands, respectively.

EEG Power Spectrum

Power spectra were calculated from the down-sampled EEG (512 Hz) using a Hanning window (FFT resolution: 0.125 Hz) in Spike2 (Cambridge Electronic Design). Spectral power density across behavioral states (REM, NREM) and experimental conditions (23°C, TNZ warm) were calculated as follows: First, for each animal and behavioral state, we averaged power spectra across 8 representative bouts per animal in each experimental condition. To determine any potential warm T_a effects on EEG power spectra, these representative bouts were selected from two successive REM and NREM sleep bouts occurring during the warmest peak of the four TNZ warm phases (total of 8 bouts per mouse). For the constant T_a baseline recording, two successive REM and NREM sleep bouts were chosen by matching the closest circadian time for each pair of bouts in the TNZ warm phases with that in the baseline condition. For normalization across animals and subsequent statistical comparisons, the spectral power density values in each bin were then divided by the maximal power within the 0.5-20-Hz frequency range across experimental conditions. Power ratios during REM (Theta/Delta) and NREM (Delta/Theta) were calculated from the averaged summed raw power in each frequency band (Delta: 1-4 Hz; Theta: 6-9.5 Hz) across bouts. Peak frequency for periods of REM (Theta) and NREM (Delta) were defined as the bin in the power spectra with the maximal value within each frequency range. To assess temperature-dependent differences in EEG parameters, we compared for each state with power in each frequency range, power ratio, or peak frequency as the repeated-measure.

Immunohistochemical labeling

To determine the specificity of viral targeting within LH neurons, MCH-cre mice transduced with either AAV2-EF1α-DIO-ChR2-eYFP (ChR2 group), AAV2-EF1α-DIO-ArchT3.0-eYFP (ArchT group) or AAV2-EF1α-DIO-eYFP (YFP control group) were perfused transcardially (PBS + 4% paraformaldehyde) under deep anesthesia approximately 35-40 days after virus injection. Brains were postfixed at 4°C for 24h in formaldehyde (4%), after which, the brains are cryoprotected in a sucrose solution (30%) for an additional 48 hr at 4°C. Finally, the brains were frozen by immersion in methyl butane (surrounded by dry ice) and conserved at −80°C until further processing.

Double immunohistochemistry was performed to identify neurons immunoreactive for YFP and MCH. Each brain was sectioned at 35 μm using a cryostat (Leica Microsystems), and slices were collected in PBS with 0.1% azide, blocked (4% BSA +0,1% PBS Triton-X) for 1 h at room temperature and then incubated with rabbit anti-GFP (1:5000, Ab 290, Abcam) and goat anti-MCH primary antibodies (1:500, SC-14509, Santa Cruz) for 48 hr at 4°C. After washing in PBS-T (PBS+0.1% Triton-X), sections were incubated with secondary antibody donkey anti-rabbit (1:500, Alexa Fluor 488, A21206, Life technologies) and donkey anti-goat (1:1000, Alexa Fluor 555, A21432, Life Technologies) for 1 h at room temperature. Sections were washed again with PBS-T and PBS, and then mounted onto glass slides (Flouromount Aqueous Mounting Medium, Sigma-Aldrich, St Louis, MO, USA). Using a fluorescence microscope, targeting efficiency was quantified.

QUANTIFICATION AND STATISTICAL ANALYSIS

Statistical Analyses

Mice underwent two recordings for each experimental condition. Statistical analyses were performed comparing the means from each mouse from the three recording conditions, i.e., a control condition at constant temperature (23.0 ± 1.0°C) and the aggregate of the TNZ warm and TNZ cool conditions. For the optogenetic experiments, means from each animal from three recording conditions were also compared for statistical purposes, i.e., control recordings and optical illumination recordings at constant temperature (23.0 ± 1.0°C), as well as optical illumination recordings during the TNZ warm condition.

All statistical analyses were performed using GraphPad Prism version 7.04 (GraphPad, USA). Two-way repeated-measures ANOVA were used for multiple comparisons or a two-tailed Student's t test for two sample comparisons. Post hoc ANOVA comparisons were followed by Sidak's Multiple Comparison Test. Data are presented as the mean ± SEM p values < 0.05 were considered to indicate statistical significance.

DATA AND SOFTWARE AVAILABILITY

Sleep-wake datasets are available upon request.

Current Biology, Volume *29*

Supplemental Information

Dynamic REM Sleep Modulation by Ambient Temperature and the Critical Role of the Melanin-Concentrating Hormone System

Noëmie Komagata, Blerina Latifi, Thomas Rusterholz, Claudio L.A. Bassetti, Antoine Adamantidis, and Markus H. Schmidt

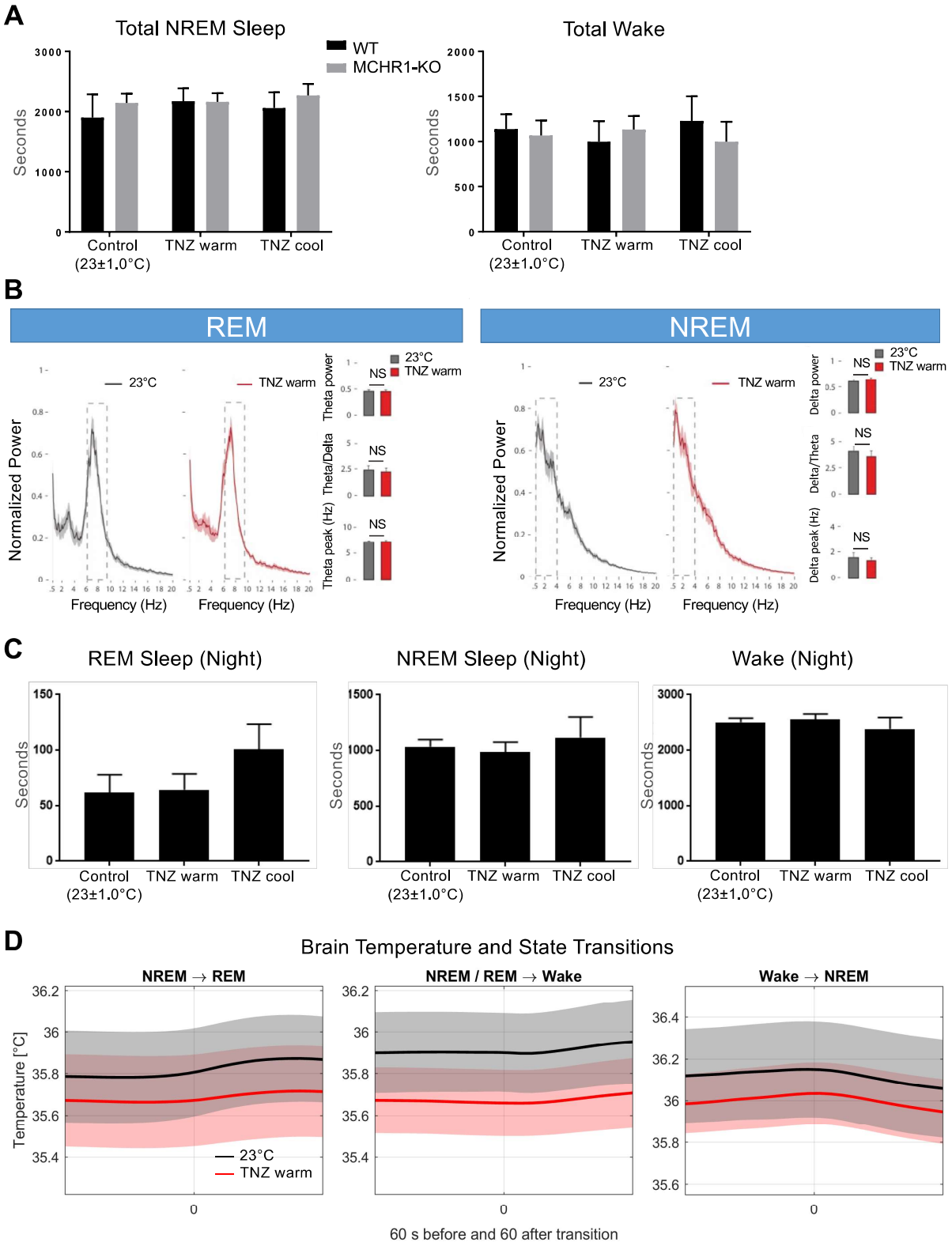

Figure S1. Effects of warm T_a pulsing on WT and MCHR1-KO mice, Related to Figure 1.
(A) Warm T_a pulsing demonstrated no significant effects on NREM sleep or wake durations.
(B) Analyses of EEG power spectra, power ratios, and peak frequencies showed no differences between the control condition at 23°C and the TNZ warm phase. Results from REM sleep and NREM sleep are

shown. Analyses for REM sleep included theta power, theta/delta ratio and peak theta frequencies, and, for NREM sleep, delta power, delta/theta ratio and peak delta frequencies (see Methods for description of analyses).
(**C**) Four bouts of warm T_a pulsing presented only during the middle of the active (night) circadian phase in WT mice (n=6) using the identical protocol for daytime T_a manipulation failed to show any significant effects from nighttime T_a warming on REM sleep, NREM sleep or wakefulness.
(**D**) Brain temperature (T_b) analyses showing no significant differences between the constant 23°C condition and the TNZ warm phase during state transitions. Data show T_b 60 sec before and 60 sec after behavioral state transitions.
Two-way repeated measures ANOVA were used for multiple comparisons or a two-tailed Student's t-test for two sample comparisons. Post-hoc ANOVA comparisons were followed by Sidak's Multiple Comparison Test. Data are presented as the mean ± SEM.

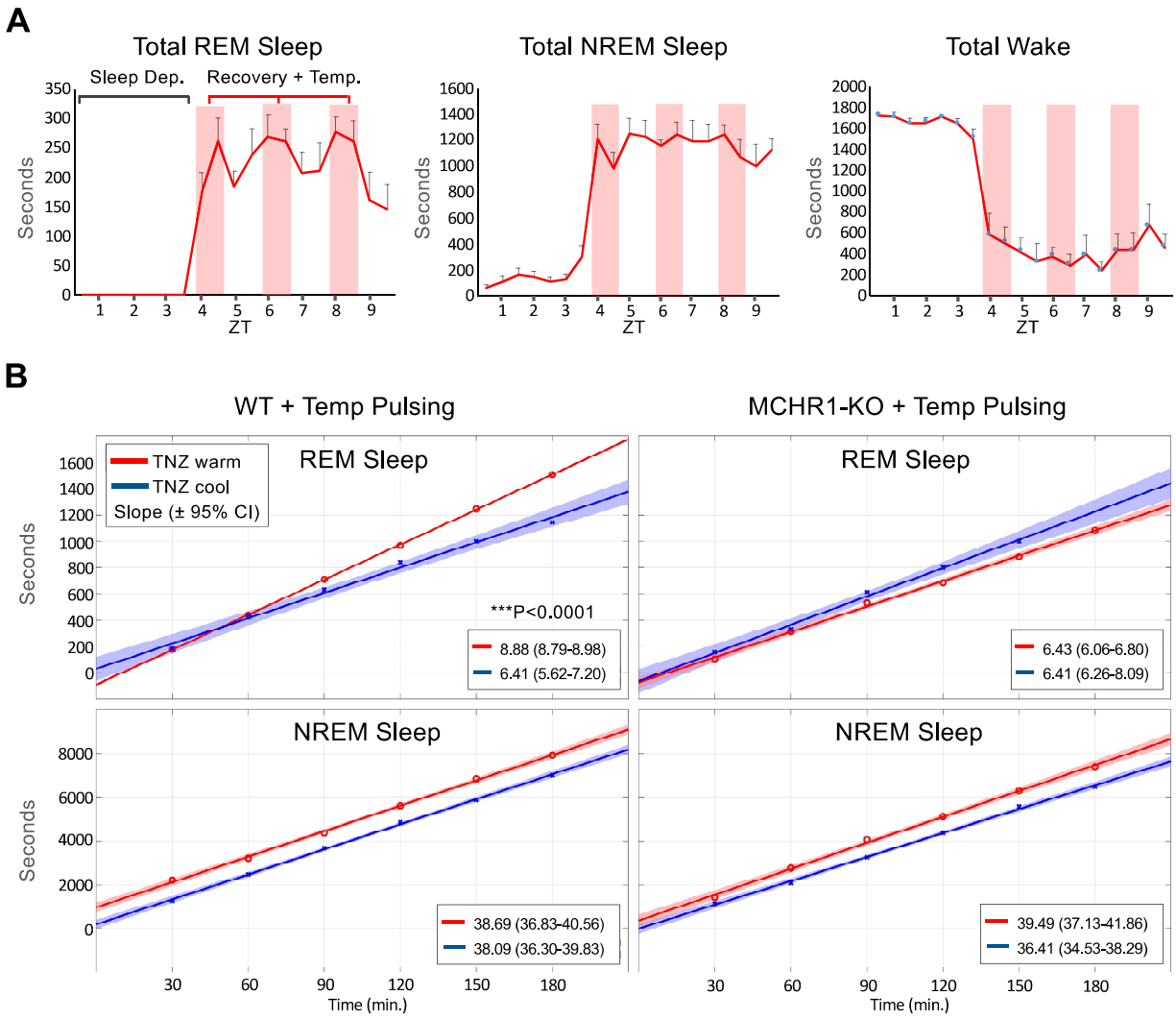

Figure S2. Effects of sleep deprivation on recovery sleep as a function of T_a, Related to Figure 2.
(A) Data from WT mice (n=8) showing the durations of either REM sleep, NREM sleep or Wake in 30-min bins during the four hours of sleep deprivation (ZT 0-4) and the first 6 hours of recovery sleep (ZT 6-10) which included three bouts of warm T_a pulsing performed at 2 hours intervals at ZT 4, 6, and 8. These data show a dynamic and consistent ability of WT mice to increase REM sleep specifically across all three of the TNZ warm phases and to subsequently decrease REM sleep during the TNZ cool phases. There were no similar specific T_a dependent effects noted for NREM sleep or wakefulness.

(**B)** The slope of cumulation (s/min) for REM sleep was significantly greater in WT mice during the TNZ warm phases compared to the TNZ cool phases (Liner regression for slope comparison $F_{(1,8)} = 74.31$, $p<0.0001$). Although the total duration of NREM sleep during recovery was increased in the first hour with T_a warming (see Fig. 2J in main text), the slope of cumulation for NREM sleep in WT mice was unchanged comparing the TNZ warm and cool phases. No differences in the slope of cumulation for either REM sleep or NREM sleep were observed in MCHR1-KO mice. Method: Linear regression was performed on average data across mice, cumulated across time for the warm and cold phase separately. The slope and intercept were obtained by MATLAB function nlinfit, which uses the Levenberg-Marquardt nonlinear least squares algorithm. The 95-% confidence interval of the slopes was calculated by MATLAB function nlparci. Additionally, we calculated the 95-% confidence interval of the predictions (fitted line) with MATLAB function nlpredci.

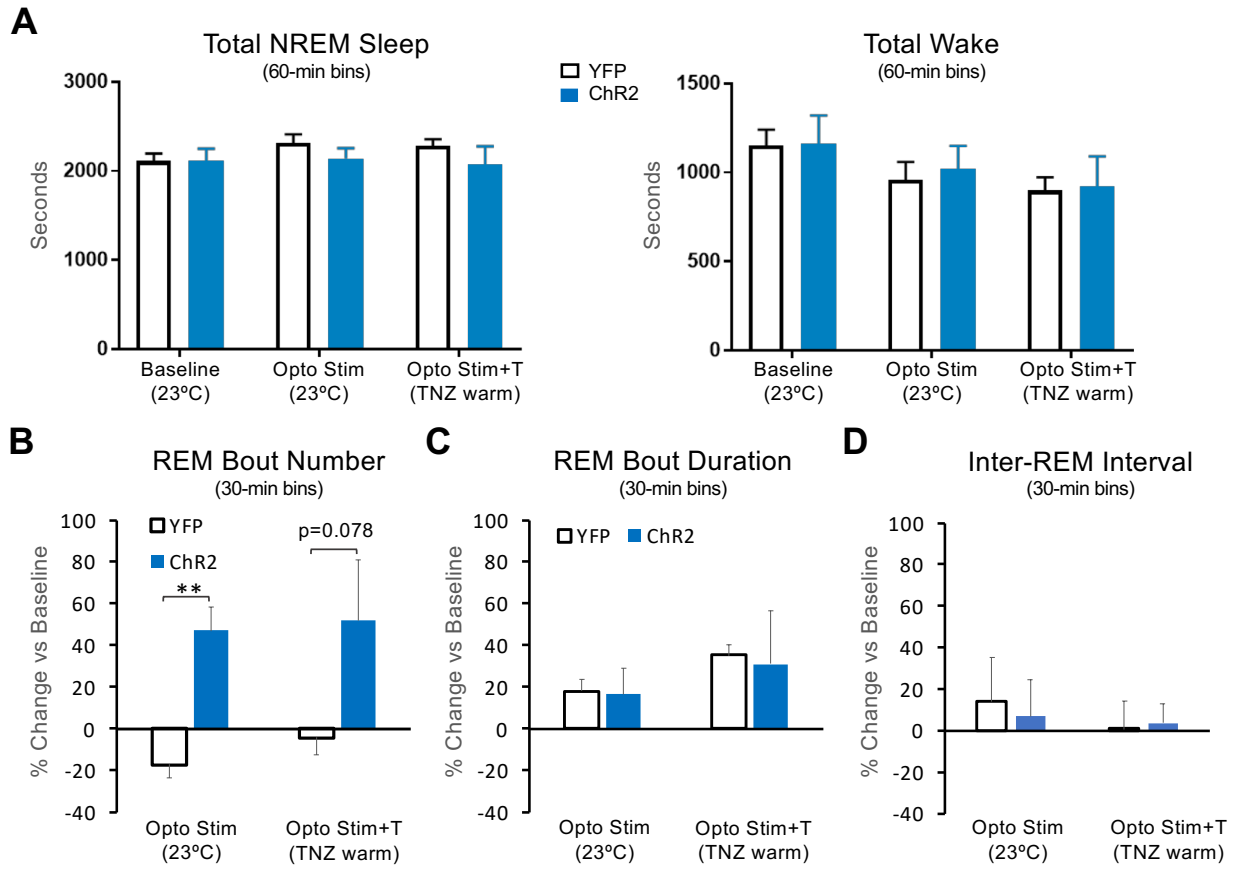

Figure S3. Effects of optical MCH activation in ChR2 and YFP mice, Related to Figure 3.
(A) Neither optical stimulation nor T_a condition showed significant effects on NREM sleep or wakefulness durations for either the YFP (n=7, white) or the ChR2 (n=7, blue) groups.
(B-D) Analyses of REM sleep bout number (B), REM sleep bout duration (C) and inter-REM intervals (D) demonstrated that MCH optical stimulation alone (Opto Stim condition) in the ChR2 group (blue) lead to a significant increase in REM sleep bout number and a similar trend with the addition of T_a warming (Opto Stim+T condition). The percent change in REM sleep bout durations (C) were highly variable in the ChR2 group. During T_a warming, for example, the YFP group showed a significant increase in REM sleep bout duration (**$p<0.01$, student's t-test) and with a tendency for increased bout durations in the ChR2 group, but with no significant differences between these two groups of mice. No consistent or significant changes were observed for inter-REM intervals (D) in either group.
Unless specified otherwise, data were analysed using repeated measures 2-way ANOVA and post-hoc Sidak's comparison test. Data are means ± SEM.

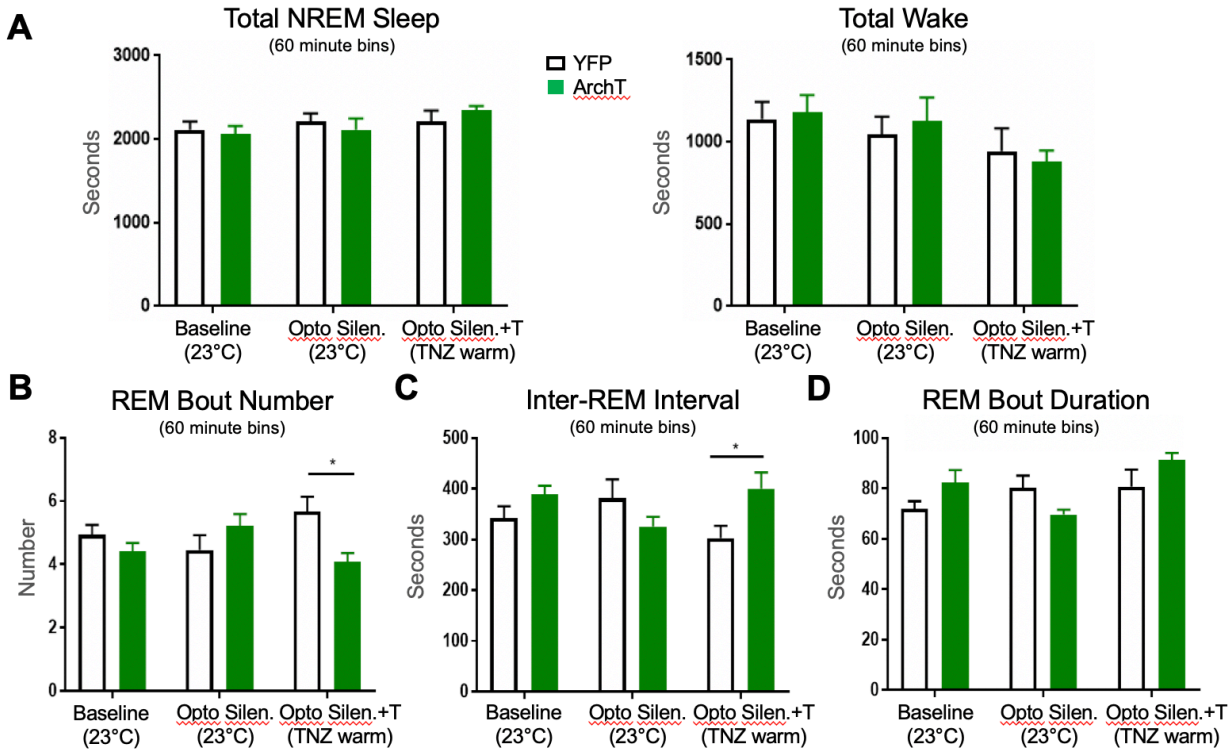

Figure S4. Effects of optical MCH silencing in ArchT and YFP mice, Related to Figure 4.
(A) Neither optical silencing nor T_a condition showed significant effects on NREM sleep or wakefulness durations for either the YFP (n=6, white) or the ArchT (n=7, green) groups.
(B-D) A two-way repeated measures ANOVA with post-hoc Sidak's comparisons (*$p<0.05$) showed that the Opto Silen+T condition was associated with a significantly greater REM sleep bout number for the YFP group compared to ArchT mice (B). A similar analysis showed significantly shorter inter-REM intervals for the Opto Silen+T condition in YFP compared to the ArchT groups (C). There were no significant effects on mean REM sleep bout durations between YFP and ArchT mice across conditions. Note: Although each bout of optical silencing occurred for only 30 minutes in duration, the TNZ warm phase was 60-minutes in duration. Given the lack of significant differences noted between the first 30-min bins with optical silencing and the second 30-min bin without optical silencing (data not shown), data were pooled for the 60-min bin analyses to evaluate potential differences during T_a warming between the YFP and ArchT groups.